Environmental Chemistry and Ecotoxicology 8 (2026) 1256–1274

Contents lists available at ScienceDirect

Environmental Chemistry and Ecotoxicology

journal homepage: www.keaipublishing.com/en/journals/environmental-chemistry-and-ecotoxicology/

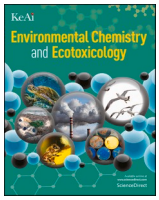

Research Paper

The sustainable synthesis of functionalized magnetic carbon nanotube adsorbent derived from steel waste for high-efficiency sequestration of tetracycline: Optimization, kinetics, isotherms and regeneration performance

Kamil Kayode Katibi [a,c,*], Rabaah Syahidah Azis [a,b,*], Ibrahim Garba Shitu [d], Ismayadi Ismail [b], Muhammad Aliyu [b,h], Nor Kamilah Saat [a], Nurul Huda Osman [a,b], Abiodun Abdulhameed Amusa [e], Raphael Terungwa Iwar [f], Abba Mohammed Umar [g]

[a] Department of Physics, Faculty of Science, Universiti Putra Malaysia, 43400 Serdang, Selangor, Malaysia
[b] Institute of Nanoscience and Nanotechnology (ION2), Universiti Putra Malaysia, 43400 Serdang, Selangor, Malaysia
[c] Department of Food and Agricultural Engineering, Faculty of Engineering and Technology, Kwara State University, Malete, 23431 Ilorin, Nigeria
[d] Department of Physics, Faculty of Science, Sule Lamido University, 700271 Kafin Hausa, Jigawa State, Nigeria
[e] Department of Chemical Engineering and Sustainability, Kulliyyah of Engineering, International Islamic University Malaysia (IIUM), Jalan Gombak, 53100 Kuala Lumpur, Malaysia
[f] Department of Agricultural and Environmental Engineering, College of Engineering, Joseph Sarwuan Tarka University, 970101 Makurdi, Nigeria
[g] Department of Agricultural and Bioenvironmental Engineering, Federal Polytechnic Mubi, Mubi 650221, Nigeria
[h] Department of Chemical Technology, Faculty of Science, Chulalongkorn University, Bangkok 10330, Thailand

ARTICLE INFO

Keywords:
Magnetic carbon nanotubes
Steel waste
Tetracycline removal
Adsorption optimization
Regeneration
RSM

ABSTRACT

Antibiotic pollution from tetracycline (TC) poses severe environmental and public health hazards. This study investigates the synthesis, characterization, and adsorptive performance of sustainable, magnetically recoverable functionalized multi-walled carbon nanotubes (FMWCNTs) adsorbent catalyzed by steel-mill waste. The adsorbent exhibits superior surface area (385 m^2/g), mesoporosity (2.2 nm), and superparamagnetic behaviour (30 emu/g), enabling efficient TC adsorption and facile recovery. Optimization using response surface methodology yielded 98.7% TC removal under optimal conditions (400 mg/L FMWCNTs, 45 mg/L TC, pH 6.5, 23 min). Adsorption followed pseudo-second-order kinetics and Langmuir isotherm (maximum capacity: 21.7 mg/g at 303 K), with thermodynamic analysis indicating a spontaneous, endothermic, and entropy-driven process. The adsorbent material retained 87% efficiency after four regeneration cycles and achieved over 90% TC removal from simulated municipal effluent. Adsorption mechanisms included π-π interactions, hydrogen bonding, electrostatic attraction, and surface complexation. These findings demonstrate the promising potential of low-cost, regenerable FMWCNTs as practical adsorbents for antibiotic-polluted water.

1. Introduction

The extensive utilization of antibiotics in surface and groundwater systems is rapidly worsening ecological and public health concerns. Tetracycline (TC), which is an extensively applied antibiotic in human and veterinary medicine [1], frequently released into aquatic ecosystems through excretion, indiscriminate disposal, and agricultural runoff [2]. Detected at concentrations ranging from ng/L to over 5 mg/L in surface waters and up to 3170 μg/L in wastewater [3].TC contributes to the growth of antibiotic-resistant bacteria and causes ecotoxicological hazards [4]. Emerging reports also indicate a potential connection between prolonged TC exposure and escalated cancer risk, though this remains under investigation [5]. Its recalcitrant and high solubility make TC difficult to remove using conventional wastewater purification systems, highlighting the need for more effective remediation strategies [6].

To address the drawbacks of conventional treatment strategies, various approaches for TC removal have been explored, including

* Corresponding authors at: Department of Physics, Faculty of Science, Universiti Putra Malaysia, 43400 Serdang, Selangor, Malaysia.
E-mail address: rabaah@upm.edu.my (R.S. Azis).

https://doi.org/10.1016/j.enceco.2026.02.006
Received 3 December 2025; Received in revised form 12 February 2026; Accepted 13 February 2026
Available online 18 February 2026

chemical oxidation [7], photodegradation [8], membrane filtration [9], advanced oxidation processes [10], and bioremediation [11]. While these approaches have demonstrated good performance, many are hampered by increased operational costs, the generation of secondary pollutants, excessive sludge production, and complex configurations [12].

Adsorption is broadly favoured for antibiotic sequestration because of its low cost, simplicity in design and operation, and superior performance [13,14]. While conventional adsorbents such as activated carbon, zeolites, and biochar show promise [15–18]. Their large-scale application is undermined by poor regeneration, high costs, and recovery issues [19]. Successive operational cycles often degrade performance due to fouling, secondary pollution, and other factors. Further drawbacks, such as non-magnetic nature, limited selectivity, and instability in complex water systems, have stimulated interest in advanced nanocomposites [20]. However, many still face challenges related to synthesis complexity, rising cost, and scalability [21]. To address the increasing demand for efficient and sustainable water purification, there is an urgent need to develop inexpensive, scalable, regenerable, and magnetically separable adsorbents capable of preserving performance under practical conditions [20].

Recent innovations have focused on developing advanced adsorbents, such as MOF-based materials [22], liquid-waste-derived magnetic porous carbon materials [23] and valorized agro-industrial wastes [24]. These materials have demonstrated improved antibiotic adsorption performance; however, many lack integrated regeneration evaluation, rely on synthetic or expensive precursors, or present challenges during magnetic separation and in real-world applications. This suggests the need for multifunctional adsorbents that combine high-performance adsorption, sustainable sourcing, magnetic recoverability, and reusability, which are rarely co-incorporated in a monolithic system.

To overcome the limitations of conventional and advanced adsorbents, attention has increasingly focused on carbon-based nanomaterials, such as multi-walled carbon nanotubes (MWCNTs), which are known for their abundant surface area, tunable functionalities, and strong affinity for pharmaceutical pollutants, including TC [4]. Undesirably, their broader application is hindered by the use of synthetic precursors and high production costs. To address this, we propose a novel strategy: synthesizing functionalized MWCNTs from steel mill-scale waste, a widely available, iron-rich byproduct of steel manufacturing. This approach reduces production costs while advancing circular-economy goals by transforming industrial waste into valuable nanomaterials. The iron content in mill scale serves as a catalyst for MWCNT growth via chemical vapour deposition, yielding magnetically responsive adsorbents that allow easy separation and recovery. By exploring surface functionalization, magnetic separability, and waste valorization, this work offers a scalable, sustainable and efficient substitute to conventional CNT synthesis, directly addressing the need for high-performance, regenerable adsorbents suitable for real-world wastewater treatment.

The FMWCNTs synthesized from steel mill-scale waste exhibit a distinct combination of properties not typically found in conventional or advanced adsorbents. Their superparamagnetic properties facilitate rapid magnetic separation, addressing the recovery challenge posed by powdered carbon materials. Acid oxidation increases surface area and mesoporosity, stimulating TC uptake via robust adsorbent-adsorbate interactions. Notably, the nanoadsorbents maintain remarkable removal efficiency over successive regeneration cycles, demonstrating their operational and economic viability. These unique properties position them as promising candidates for scalable water purification, offering facile recovery, reusability, and longstanding stability.

Despite progress in antibiotic remediation technologies, several studies have integrated aspects such as magnetic recoverability, regeneration, and mechanistic insights; however, relatively few have consolidated these features into a single, scalable adsorbent system derived from industrial waste streams [25,26]. Most existing research focuses either on demonstrating high removal efficiency or developing novel materials, but not both in a consolidated, scalable system [27,28]. Also, limited efforts have focused on valorizing large-scale industrial waste for synthesizing magnetic carbon-based adsorbents while addressing key functional metrics, such as regeneration and adsorption mechanisms. For instance, while biopolymer-based composites [29] and industrial waste-derived materials [30] have shown promise, they often lack in-depth regeneration studies or efficient magnetic recovery. Analogously, advanced materials such as Fe-BTC MOFs [31], surfactant-modified nanoparticles [32], and carbon composites [33] show high adsorption performance but are rarely evaluated over multiple cycles, optimized, or modelled for adsorption kinetics and thermodynamics. These drawbacks reveal a clear research gap: the need for inexpensive, environmentally sustainable, and magnetically recoverable adsorbents with robust performance and mechanistic clarity under real-world water purification conditions. Steel mill scale is a conventional solid byproduct produced during hot-rolling of steel, typically containing iron oxides such as Fe_3O_4, Fe_2O_3, and FeO. It accounts for 1–2% of overall steel production and is often used as industrial waste, raising concerns about waste disposal and environmental management [34,35]. Interestingly, its superior iron content and magnetic properties make it a viable precursor for the synthesis of magnetic nanomaterials. Recent studies have explored its potential for various applications, especially for producing inexpensive, sustainable magnetic adsorbents [14,16]. In this work, we utilize steel mill scale waste as a catalytic iron source for the synthesis of functionalized magnetic carbon nanotubes, congruent with resource valorization and circular economy principles.

To address these gaps, this study proposed a magnetically recoverable nanoadsorbent synthesized from steel mill-scale waste via catalytic chemical vapour deposition. The iron-loaded waste serves as an inexpensive precursor for producing FMWCNTs with oxidized surfaces and embedded magnetic domains, improving adsorption performance while enabling facile recovery. The material was thoroughly characterized to correlate structural properties with adsorption performance, and TC removal was optimized using response surface methodology supported by kinetic, isotherm, thermodynamic, and diffusion analyses. By incorporating industrial waste valorization with magnetic CNT synthesis and statistically validated process optimization, this work advances beyond conventional CNT-based adsorbents and presents mechanistic, surface-level insight under practical operational conditions. The integrated approach addresses key scalability challenges in antibiotic adsorption and aids the development of sustainable, circular-economy-oriented wastewater purification technologies.

2. Materials and methods

2.1. Chemicals

Raw mill-scale waste obtained from a steel manufacturing plant in Serdang, Malaysia, was used as the iron-rich precursor. Methanol (≥ 99.9% purity), hydrochloric acid (38% purity), and sulfuric acid (98% purity) were supplied by Sigma-Aldrich (Germany). Sodium hydroxide pellets (≥99% purity) were purchased from J.T. Baker (Thailand). Analytical-grade Tetracycline hydrochloride (≥98% purity) was sourced from Mosaaj Pharmaceuticals (Ilorin, Kwara, Nigeria). All chemicals were used as received without further purification. De-ionized water (18.2 MΩ cm) was produced on a Millipore Alpha-Q system, and all aqueous solutions were prepared with this water. Tetracycline is a very water-soluble, amphoteric antibiotic characterized by multiple ionizable functional groups (pKa = 3.3, 7.7, and 9.7) and a molecular size of approximately 1.2 × 0.75 nm, properties that strongly influence its environmental behaviour and adsorption performance (Table S1).

2.2. Preparation of the adsorbent

The FMWCNTs were synthesized in two stages: (i) preparation of

nano-Fe_3O_4 catalyst from mill-scale waste and (ii) growth of MWCNTs using chemical vapour deposition (CVD) procedure.

2.3. Stage 1: Fe_3O_4 catalyst preparation

Mill scale waste (120 g) was dry-milled for 48 h in a planetary ball mill (Fritsch Pulverisette 6) at 300 rpm using stainless-steel media (10 mm diameter) with a ball-to-powder mass ratio of 10:1. A milling duration of 48 h was adopted to stimulate adequate mechanical activation and dispersion of the iron oxide precursor prior to CVD growth, in line with previously reported optimization studies on iron-based catalysts for nanocarbon synthesis [36,37]. The ground powder was rinsed with de-ionized water, filtered and dried at 110 °C overnight. Magnetic separation isolated the Fe_3O_4 fraction, which was further purified by Curie-temperature separation to remove non-magnetic phases. The concentrate was dispersed in 0.1 M HCl (solid: liquid = 1:20 *w/v*) to minimise agglomeration, then dried at 100 °C. A 6 h high-energy milling step (Spex 8000 M shaker mill, 950 rpm) yielded nanocrystalline Fe_3O_4 with abundant surface defects that enhance catalytic activity. A one-day milling protocol (BM-1 d) was selected as the optimum compromise between size reduction and crystallinity, in line with [38].

2.4. Stage 2: CVD growth of MWCNTs

Approximately 1.0 g of the Fe_3O_4 nanocatalyst was placed in a horizontal tube furnace at the centre of a high-purity alumina tube. After evacuation, the tube was purged with ultra-high-purity argon (99.999%, 250 sccm) and heated to 900 °C at 10 °C min^{-1}. Ethanol (99.9%) pre-heated to 80 °C served as the main carbon source; ethylene (99.995%, 150 sccm) and hydrogen (99.999%, 250 sccm) were co-fed for two hours to enhance carbon supply and maintain a reducing atmosphere. The furnace was then cooled to ambient temperature under argon to preserve nanotube integrity.

2.5. Purification and surface functionalization

Pristine MWCNTs (0.20 g) were refluxed in a 3:1 (*v*/v) mixture of concentrated H_2SO_4 (18 M, 9 mL) and HNO_3 (16 M, 3 mL) and ultrasonicated at 45 °C for two hours to dissolve residual Fe species and amorphous carbon [39]. This acid oxidation grafted –OH and –COOH groups onto the nanotube surface, increasing aqueous dispersibility and affinity for tetracycline. The suspension was washed with de-ionized water to pH:7, filtered through a 0.22 µm PVDF membrane, and oven-dried at 110 °C for 12 h. The purified FMWCNTs were stored in airtight glass vials. The overall yield of purified FMWCNTs was 6.3 g per 100 g of mill scale, corresponding to a mass-conversion efficiency of 6.3%. Fig. 1 schematically illustrates (a) the conversion of mill-scale waste to Fe_3O_4 nanoparticles and (b) the CVD setup used for FMWCNT synthesis. (See Scheme 1.)

2.6. Adsorbent measurement details

The structural morphology of the synthesized adsorbent was assessed using a NovaNano 230 Field-Emission Scanning Electron Microscope (FESEM) at 5–15 kV, with magnification ranges between 10,000 × −100,000×, while the elemental compositions and EDX spectra of the

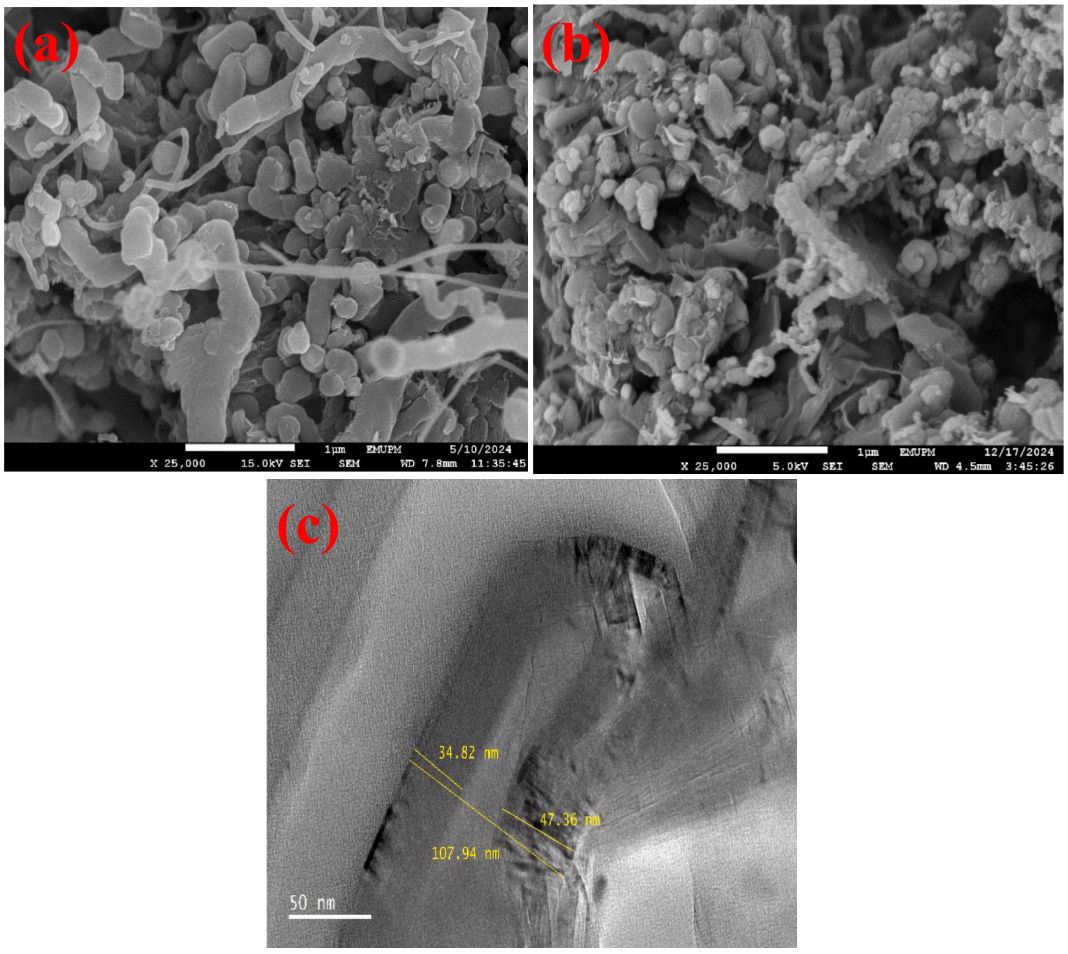

Fig. 1. FESEM image of FMWCNTs before TC adsorption (a), FESEM image of FMWCNTs after TC adsorption (b), EDX spectrum of FMWCNT (c), TEM image of FMWCNT (d).

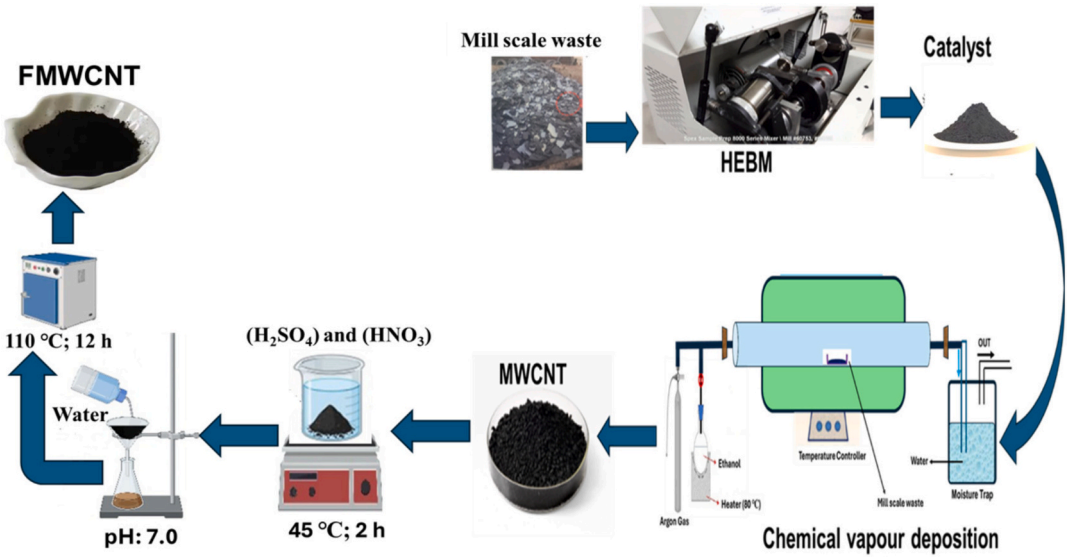

Scheme 1. Schematic illustration of the synthesis procedure of Functionalized Multiwalled Carbon Nanotube Adsorbent Material.

adsorbent were ascertained via energy dispersive spectroscopy (EDS) utilizing the Bruker/Quanta 200 system, Westerville, OH, USA, resolution 127 eV, by means of a working distance of 8–10 mm. TEM micrographs were acquired using a JEOL JEM-2100F microscope operating at 200 kV to study tube morphology together with internal wall structures.

X-ray diffraction (XRD) was employed to characterize the crystal structure and phase composition of the synthesized FMWCNT. This analysis was conducted using a Philips X-ray diffraction expert diffractometer with Cu Kα radiation (λ = 0.154 nm) over a 2θ range of 10 to 70°, with a 2θ step size of 0.033° and a counting time of 5 s per step. The magnetic hysteresis characteristics of the MWCNT adsorbent were investigated using a vibrating sample magnetometer (VSM, LakeShore7404) under an external magnetic field ranging from −10,000 Oe to 10,000 Oe. Furthermore, the specific surface area of the adsorbent was determined using the Brunauer-Emmett-Teller (BET) method with the Micromeritics II PLUS instrument in the USA, employing nitrogen adsorption-desorption isotherms, and the NOVA2020e automatic surface area and porosity analyser. Samples (adsorbent) were degassed under vacuum at 100 °C for 12 h prior to nitrogen adsorption measurements. Furthermore, Fourier Transform Infrared (FTIR) spectroscopy was utilized to provide insights into the functional groups present on the FMWCNT adsorbent material. Employing the Bruker-Tensor 27 IR instrument following the standard KBr-pellet technique within the spectral region of 4000–400 cm^{-1} (Bruker Tensor 27, KBr pellet method) at a resolution of 2 cm^{-1} facilitated the identification of FTIR spectra of the adsorbent.

2.7. Batch experimental procedure

This research focused on assessing TC adsorption on FMWCNT through a series of batch experiments. All tests were performed using 100 mL polypropylene Erlenmeyer flasks containing 50 mL of aqueous TC solution. Flasks were agitated at 160 rpm on an orbital shaker, and the temperature was maintained at 25 ± 1 °C. The tests were designed to examine the optimal conditions for TC adsorption by varying key independent variables: initial TC concentration (10–100 mg/L), adsorbent dosage (0.1–1.0 g/L), pH (3–9), and contact time (10–120 min). The experimental ranges of the independent variables were selected based on generally reported conditions for TC adsorption and practical relevance to wastewater purification systems [40]. The initial TC concentration (10–100 mg/L) covers a broad loading range frequently applied in adsorption studies, while the adsorbent dosage (0.1–1.0 g/L) allows evaluation of binding-site availability under realistic liquid-solid ratios [41]. The pH range (3–9) spans the dominant protonation states of TC and surface charge variation of carbon-based adsorbents, and the contact time (10–120 min) captures both rapid adsorption and equilibrium behaviour typically observed for CNT-based materials [42].

A full factorial experimental design with three levels for each factor (−1, 0, +1) was employed to systematically evaluate their effects. All adsorption experiments were conducted in triplicate, and results are reported as mean ± standard deviation, with experimental errors consistently below ±2%. Model validation was performed using adsorbent dosages of 200, 300, and 400 mg/L.

Upon completion of the adsorption, samples were filtered using 0.22 μm PVDF membranes and centrifuged to ensure complete elimination of suspended solids. TC concentrations were determined utilizing UV–Vis spectrophotometry at 355 nm using a five-point calibration curve ($R^2 \geq 0.999$), with selected samples further validated by reverse-phase HPLC (C18 column, UV detection at 355 nm) to confirm analytical accuracy. Calibration standards (0–100 mg/L) demonstrated good linearity ($R^2 > 0.995$). All solutions were adjusted to an ionic strength of 0.10 M using KCl, and pH was controlled with 0.1 M HCl or NaOH and monitored using a calibrated pH meter. The error in per cent removal was consistently less than ±2%. Also, the removal efficacy of TC was confirmed through three repeated trials conducted under optimal conditions, as assessed by the Central Composite Design (CCD). The TC adsorption percentage of the adsorbents was computed using Eq. (1) [15]:

$$Adsorption\ (\%) = \left(\frac{C_i - C_f}{C_i}\right) \times 100 \quad (1)$$

Where C_i and C_f represent the initial equilibrium and final concentrations of TC (mg/L) respectively. The TC adsorption capacity was computed using the mass balance Eq. (2) [16]:

$$q_e = (C_i - C_e)V/m \quad (2)$$

In this context, C_e depicts the final and equilibrium concentration of TC (mg/L), q_e represents the adsorption capacity (mg/g), m is the mass of MWCNT (g), and V is the volume of the TC solution (L).

2.8. Optimization of adsorption process using experimental design

A central composite design (CCD) in the response surface methodology (RSM) framework was utilized to assess the optimal conditions for adsorption by considering the main process variables. The selection of variable ranges for RSM was guided by preliminary single-factor ex-

periments, which identified the response trends and the factor's effective ranges for TC removal. This approach aligns with recent optimization strategies reported in the literature, where initial single-variable testing helps define effective parameter ranges for multi-factorial RSM modelling [42,43]. The studied variables comprised initial concentration (A), contact time (B), pH (C), as well as adsorbent dosage (D), with a total of 30 experimental runs performed to optimize the adsorption of TC. The adsorption response, denoted as Y, was modelled as a function of these process variables, incorporating an error term (ε), as described by Eq. (3):

$$Y = f(X_1, X_2, X_3, X_4) + \varepsilon \tag{3}$$

where ε describes errors in the response measurement. The process response followed a second-order quadratic model, represented in Eq. (4).

$$Y = \beta_0 + \sum_{i=1}^{K} \beta_i X_i + \sum_{i=1}^{K} \beta_{ii} X_i^2 + \sum_{i>j}^{K} \beta_{ij} X_i X_j + \epsilon \tag{4}$$

Here, β_0 depicts the constant coefficient, β_i denotes the linear coefficients for each factor X_i, β_{ii} corresponds to the quadratic coefficient, and βij implies the interaction coefficients between the input process variables. The error term ε describes the model deviations.

The response surface was produced to analyze the actual function behaviour. The expression in Eq. (5) determined the required number of experiments (N).

$$N = 2^k(k-1) + C_o \tag{5}$$

where k accounts for the number of independent process variables, and C_0 represents the number of central points. This study examined three functional process variables (k = 3), yielding the corresponding number of experiments (N). Factor levels were coded as +1 (high), −1 (low), and 0 (central point) to standardize the analysis. Each test was performed in triplicate, with the mean values recorded.

Statistical analysis and model validation were performed using Design-Expert v12 (Stat-Ease, Inc., Minneapolis, USA). The factor levels and their respective coding are presented in Table 1. This approach systematically evaluates adsorption efficiency under controlled conditions and optimizes process variables to improve performance. All experiments were performed in triplicate to ensure reproducibility. Data are reported as mean values ± standard deviation, and error bars representing standard deviation are included in all relevant figures.

2.9. pH-speciation modelling of tetracycline

The fractional distribution of TC species (TC^{2-}, TCH_2, TCH_3^+) was computed with Visual MINTEQ v3.1 using the NIST 2019 thermodynamic database. Computations were carried out for a 1×10^{-4} M TC solution in 0.10 M KCl at 298 K, illustrating the ionic strength and temperature of the batch experiments. The pH was incremented from 2.0 to 12.0 in 0.1-unit steps. Reported pK_a values (3.33, 7.67, 9.68) [44] were validated by repeating the computation in HySS 2009; deviations were < 0.05 pH units. Protonated and deprotonated molecular structures were drawn using ChemDraw 23.0.

Table 1
Coded and actual values of independent variables employed in the design of an experimental matrix using the RSM-CCD outline.

Independent Process Variables	Units	Factor code	Level of factors		
			Low (−1)	Central (0)	High (+1)
MWCNT Dosage	g/L	A	0.1	0.55	1.0
TC Initial concentration	mg/L	B	10	55	100
pH	–	C	3	6	9
Contact time	min	D	10	65	120

2.10. Isotherm model studies

Adsorption isotherm experiments were performed to assess the equilibrium interaction between TC and FMWCNTs using batch tests with initial TC concentrations of 20–300 mg/L at 288, 298, and 308 K. Briefly, 50 mg of FMWCNT was added to 50 mL of TC solution in sealed 100 mL Erlenmeyer flasks and agitated at 160 rpm for 24 h to ensure equilibrium. After adsorption, the adsorbent was separated magnetically, and the supernatant was filtered using a 0.22 μm PVDF membrane. Residual TC concentrations were quantified by UV–Vis spectrophotometry at 355 nm. All experiments were carried out in triplicate, and mean values were used for analysis. The equilibrium adsorption capacity q_e (mg/g) was computed using Eq. (2). The acquired data were fitted to nonlinear Langmuir and Freundlich isotherm models.

The Non-linear Langmuir Model Equation used is expressed in Eq. (6):

$$q_e = (q_{max} \times bC_e)/(1 + bC_e) \tag{6}$$

Where q_{max} (mg/g) depicts the maximum monolayer adsorption capacity, and b (L/mg) represents the Langmuir adsorption constant.

Similarly, the non-linear Freundlich model was computed using Eq. (7):

$$q_e = K_F C_e^{\frac{1}{n}} \tag{7}$$

where k_F denotes the Freundlich adsorption constant, and 1/n represents an empirical parameter related to adsorption intensity. The adsorption model that provided the best fit was selected based on the coefficient of determination (R^2) and residual sum of squares (RSS).

Also, the Temkin isotherm model was applied to better understand the adsorbent-adsorbate interactions and heat of adsorption. The Temkin model assumes that the heat of adsorption declines linearly with coverage and is expressed as [16]:

$$q_e = B\ln A + B\ln C_e \tag{8}$$

where $q_e$signifies the equilibrium adsorption capacity (mg/g), $C_e$represent the equilibrium concentration (mg/L), A denote the Temkin isotherm equilibrium binding constant (L/g), and $B = \frac{RT}{b}$is related to the heat of adsorption, with R being the universal gas constant and T is the absolute temperature.

2.11. Adsorption kinetics studies

Kinetic experiments were conducted to evaluate the rate of TC adsorption onto FMWCNTs using a 20 mg/L TC solution at 298 K. Briefly, 50 mg of FMWCNT was added to 50 mL of TC solution in 100 mL Erlenmeyer flasks and agitated at 180 rpm and 26 ± 1 °C. At predetermined time intervals (0–60 min), aliquots were withdrawn, magnetically separated, and filtered through a 0.22 μm PVDF membrane to remove residual adsorbent. The remaining TC concentration was quantified by UV–Vis spectrophotometry at 355 nm. All experiments were performed in triplicate, and mean values were used for analysis. A known amount of adsorbent was added to 50 mL of the TC solution and agitated at 160 rpm. At specific intervals (0–60 min), aliquots were withdrawn, filtered, and analyzed for residual TC concentration. The experimental data were analyzed using pseudo-first-order (PFO) and pseudo-second-order (PSO) kinetic models:

The adsorption capacity at time t, denoted as qt, was computed using Eq. (9):

Pseudo-First-Order,

$$q_t = q_e\left(1 - e^{-k_1 t}\right) \tag{9}$$

Where q_t depicts adsorption capacity at time t (mg/g), k1 is the pseudo-first-order rate constant (min^{-1}), and t represents the adsorption time (min).

Pseudo-Second-Order is expressed in Eq. (9):

$$q_t = \frac{t}{\frac{1}{k_2 q_e^2} + \frac{t}{q_t}} \tag{10}$$

Where k_2 signifies pseudo-second-order rate constant (g/mg.min). The kinetic data were plotted, and the model with the highest R^2 was selected as the best fit.

In addition to pseudo-first- and pseudo-second-order kinetic models, the Weber-Morris intraparticle diffusion model was employed to assess the diffusion mechanism and determine whether intraparticle diffusion was the rate-limiting step. The model is expressed as [45]:

$$q_t = k_{id} t^{0.5} + C \tag{11}$$

where q_t(mg/g) is the adsorption capacity at time t, k_{id}(mg/g·$min^{0.5}$) is the intraparticle diffusion rate constant, and $C$is the intercept related to the boundary layer effect.

2.12. Adsorption thermodynamics

To evaluate the adsorption thermodynamics of MWCNT for TC, 100 mL of the TC solution and 0.2 g of the adsorbent were put into a 250 mL conical flask. The mixtures were subjected to agitation at a speed of 160 rpm, pH 6, for a 60 min adsorption period at temperatures ranging from 298.15 K to 313.15 K in a temperature-controlled incubator shaker (Excella E24 Incubator shaker series, USA). The thermodynamic variables, including enthalpy change (ΔH), standard Gibbs free energy change (ΔG°), and change in entropy (ΔS°), were computed and summarized using the following Eqs. (12–14):

$$\Delta G_0 = -RT\ln K_L \tag{12}$$

$$K_L = \frac{q_e}{C_e} \tag{13}$$

$$\Delta S^0 = \Delta H^0 - \frac{\Delta G^0}{T} \tag{14}$$

Where ΔG° represents standard Gibbs free energy change, ΔS° signifies entropy change, ΔH° is the enthalpy change, R denotes the gas constant (8.314 J/mol^{-1} K^{-1}), C_e is the equilibrium concentration of TC (mg/L), q_e is the quantity of TC adsorbed onto MWCNT (mg/g), and T represents the absolute temperature (K).

2.13. Regeneration and desorption studies

Desorption experiments were conducted to elucidate the TC release mechanism and evaluate adsorbent reusability. Desorption tests were performed over a pH range of 4–10 at a fixed adsorbent dosage of 300 mg/L, revealing enhanced TC release under alkaline conditions due to electrostatic repulsion.

Regeneration performance was assessed through consecutive adsorption–desorption cycles under optimized conditions. In each adsorption step, FMWCNTs (400 mg/L) were contacted with TC solution (45 mg/L) at pH 6.5 and agitated at 180 rpm for 1 h. The spent adsorbent was magnetically separated, rinsed, and dried prior to reuse. Desorption was carried out using NaOH solutions of varying concentrations and temperatures (1 mol/L at 25 and 35 °C, and 2 mol/L at 35 °C) with stirring for 120 min. Alkaline eluents were selected based on the pH-dependent speciation of TC and surface charge behaviour of FMWCNTs; at pH values above the pH_pzc (5.19), both TC and the adsorbent surface are predominantly negatively charged, promoting electrostatic repulsion and facilitating desorption. Adsorption efficiency was monitored over four regeneration cycles.

It is noteworthy that FMWCNTs are insoluble carbon-derived nanomaterials and remain structurally stable under the investigated conditions. Prior to analysis, all suspensions were magnetically separated and filtered (0.22 μm) to remove residual particles. Control experiments confirmed negligible background absorbance at 355 nm, and selected samples were validated by HPLC to ensure that TC quantification was not affected by potential light scattering effects or leaching.

3. Results and discussion

3.1. Adsorbent measurement

3.1.1. Morphological analysis of synthesized MWCNT

Fig. 1 presents FESEM micrographs of FMWCNTs before and after TC adsorption, illustrating their morphological integrity and surface characteristics. As shown in Fig. 1a, the pristine FMWCNTs exhibit a typical entangled tubular network with smooth, clean surfaces and minimal residual impurities, indicating successful synthesis and purification. The uniform tube diameters and interconnected bundles suggest a high surface area and accessible pore network, which are favourable for adsorption. Importantly, the well-preserved morphology confirms that acid functionalization effectively modified the surface chemistry without compromising the nanotubes' structural integrity.

In contrast, Fig. 1b shows distinct morphological changes after TC adsorption. The FMWCNT surfaces are partially covered by irregular layers and particulates, attributable to adsorbed TC molecules, confirming strong surface interactions. These features support the proposed adsorption mechanisms, including π–π stacking between TC aromatic rings and graphitic CNT walls, as well as hydrogen bonding and electrostatic interactions involving oxygen-containing functional groups introduced by acid treatment. In addition, iron-based surface sites (Fe ≈ 5.30 wt%) may facilitate further surface complexation, while the slight post-adsorption aggregation likely reflects intermolecular bridging or stacking of adsorbed TC. Overall, these morphological changes highlight the role of surface functionalization in strengthening adsorbate–adsorbent interactions and enhancing adsorption efficiency.

Fig. 1c presents a TEM image of the synthesized FMWCNTs, clearly revealing the characteristic multi-walled tubular structure composed of well-ordered concentric graphitic layers surrounding a hollow core. The nanotubes exhibit inner diameters of approximately 5–10 nm and wall thicknesses of 10–15 nm, indicating dense graphitic stacking and high structural robustness. These dimensions are consistent with MWCNTs produced via CVD, confirming effective control over the synthesis parameters [46,47]. The nanotubes remain intact and uniform, with no evident tube collapse or wall distortion, indicating excellent structural preservation during synthesis and post-treatment. This confirms that acid oxidation with H_2SO_4/HNO_3 did not compromise nanotube integrity. Instead, the subtle wall irregularities and edge-plane defects observed by TEM suggest partial oxidation and surface etching, which are advantageous for adsorption by exposing additional reactive sites.

In addition, small dark contrast features distributed along and between the nanotube walls likely correspond to embedded Fe_3O_4 nanoparticles formed during catalytic growth. The well-defined tube walls and preserved hollow cores corroborate the mesoporous characteristics identified by BET analysis and support adsorption mechanisms such as π–π stacking, electrostatic attraction, and hydrogen bonding. The accessible inner channels and exposed graphitic surfaces further confirm the suitability of FMWCNTs for adsorbing large organic molecules such as TC, whose molecular dimensions are comparable to the nanotube inner diameter [48].

Thus, the TEM analysis confirms the fabrication of structurally intact, functionally active, and magnetically responsive FMWCNTs. These properties, along with the quantified dimensions and surface modifications, promise them for use as efficient, regenerable adsorbents for the remediation of antibiotic-laden wastewater.

3.1.2. Phase and structural analysis

The crystallographic structure of the synthesized FMWCNT was analyzed using X-ray diffraction (XRD), as illustrated in Fig. 2a. A broad but distinct diffraction peak was observed at $2\theta = 26^\circ$, corresponding to the (002) plane of graphitic carbon. This peak confirms the stacked carbon layers characteristic of MWCNTs and indicates a turbostratic arrangement of graphene sheets. The broadening and moderate intensity of the (002) peak indicate a partial loss of crystallinity, which is attributed to acid oxidation functionalization using HNO_3 and H_2SO_4 [49]. This treatment introduces oxygen-containing functional groups (-COOH, -OH) and surface defects, which disrupt the orderly graphitic structure without undermining the tubular framework [50].

Additional sharp peaks located at $2\theta = 35.5^\circ$ (311), 43.0° (101), and 62.8° (533) conform to the spinelle structure of Fe_3O_4 (magnetite) [51,52]. These peaks substantiate the successful incorporation of magnetic iron oxide nanoparticles derived from the mill scale during the CVD process. The presence of Fe_3O_4 peaks after functionalization indicates that the acid treatment did not weaken the magnetic crystalline phase.

In addition to crystallite size, the lattice parameter (a) of the Fe_3O_4 phase was estimated using Bragg's law and the Equation for cubic systems:

$$a = d\sqrt{h^2 + k^2 + l^2} \tag{15}$$

where *d*is the interplanar spacing calculated from the Bragg angle, and *hkl*are the Miller indices of the (311) plane, which is the most intense peak for Fe_3O_4. Using the peak at $2\theta \approx 35.5^\circ$, the computed lattice constant was 8.39 Å, which is consistent with literature values for magnetite (Fe_3O_4), confirming the formation of a spinel cubic structure. This result supports the successful incorporation of iron oxide domains into the carbon nanotube matrix. These findings align with previous studies reporting similar lattice parameters for Fe_3O_4 nanoparticles synthesized via green or waste-derived routes [17,53]. The retention of both carbon and iron oxide phases corroborates the formation of a hybrid nanocomposite with dual functionality, structural suitability for adsorption and magnetic recoverability.

The structural properties confirmed by XRD directly support the application of FMWCNTs as effective adsorbents for pharmaceutical removal. The defect-rich graphitic structure facilitates π–π interactions and hydrogen bonding, while the embedded Fe_3O_4 phase enhances magnetic separation and potential surface complexation with target molecules such as TC. Thus, the XRD results substantiate the successful synthesis of a mesoporous, magnetically active, and functionally enhanced composite, essential for practical application in environmental remediation.

3.1.3. Magnetic strength analysis

Fig. 2b presents the magnetic hysteresis loop of the synthesized FMWCNT, obtained using VSM at ambient temperature. The curve shows a narrow S-shaped hysteresis loop, indicative of superparamagnetic behaviour, with negligible coercivity (Hc) and remanence (Mr). This magnetic property is ideal for adsorbent applications, as it allows the material to magnetize rapidly in the presence of an external magnetic field and demagnetize when the field is removed, thereby preventing permanent agglomeration and facilitating redispersion [24]. The synthesized FMWCNT material exhibited a saturation magnetization (Ms) of 30 emu/g, which is considered relatively high for carbon-based magnetic nanocomposites. The results indicate that FMWCNT is sufficient to enable efficient magnetic separation from aqueous solutions [17]. The decline in Ms. is expected due to the non-magnetic carbon nanotube matrix, which dilutes the overall magnetic content while providing a high surface area for adsorption.

This balance between surface functionality and magnetization is critical in environmental remediation. The Fe_3O_4 nanoparticles embedded within the MWCNT framework not only impart magnetic responsiveness but also promote adsorption mechanisms through surface complexation or redox interactions, principally with functional groups such as carboxyl and hydroxyl introduced during acid oxidation [54]. Also, the superparamagnetic nature guarantees that the adsorbent does not retain residual magnetism, thus maintaining its structural stability and reusability over multiple adsorption–desorption cycles [55]. Therefore, the VSM results indicate that the FMWCNTs possess sufficient magnetic strength for practical magnetic separation while maintaining the surface chemistry essential for efficient TC adsorption. The combination of high saturation magnetization and surface functionalization positions the material as a strong candidate for high-performance and recyclable water treatment systems.

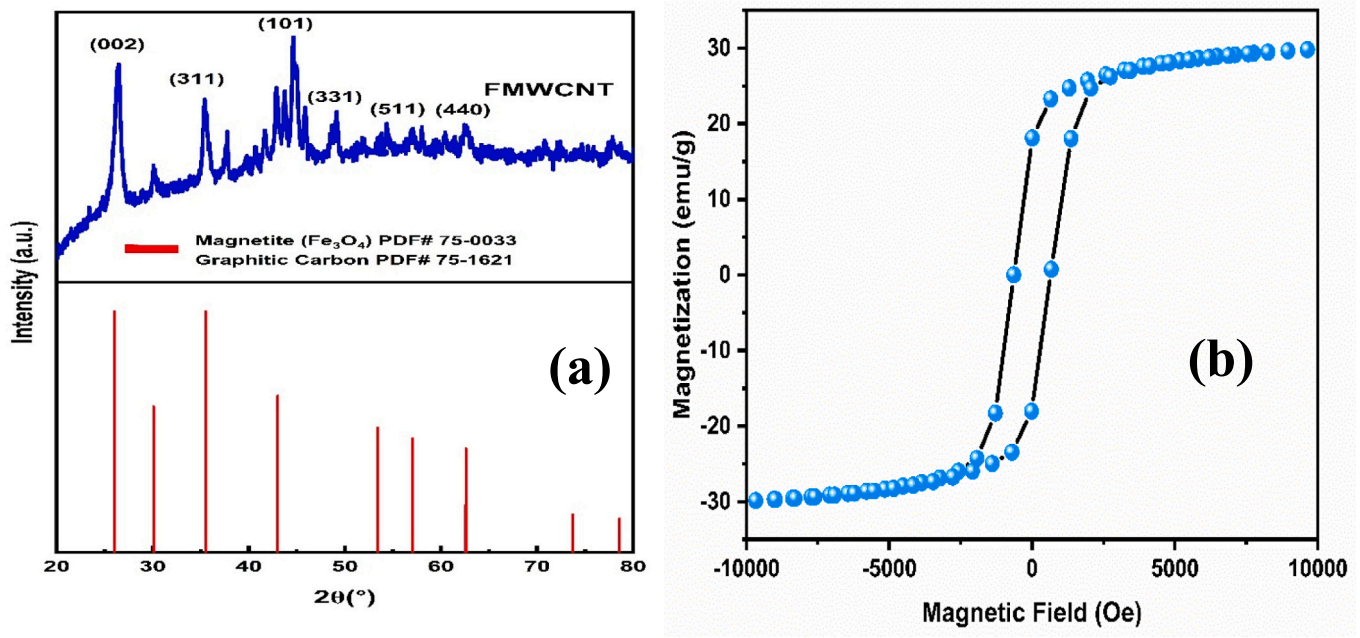

Fig. 2. XRD pattern of FMWCNT (a), Magnetic hysteresis loop of FMWCNT at room temperature (b).

3.1.4. Textural properties, porosity, and elemental composition of synthesized FMWCNT

The textural and elemental properties of the synthesized FMWCNT were investigated using N_2 adsorption-desorption isotherms and elemental analysis, with results presented in Table 3 and illustrated in Fig. 3a and b, respectively. As illustrated in Table 3, the FMWCNTs had a BET surface area of 385 m^2/g and an average pore diameter of 2.15 nm. According to IUPAC pore size classification, this pore diameter places the FMWCNTs in the mesoporous category (2–50 nm). The N_2 adsorption-desorption isotherm in Fig. 3a presents a Type IV isotherm with an H3 hysteresis loop, indicative of mesoporous materials having slit-like pores formed by plate-like particles or aggregates. This substantiates that capillary condensation occurs in mesopores, essential for efficient adsorption of large organic pollutants such as TC [41].

Similarly, the pore size distribution curve in Fig. 3b further corroborates this observation, exhibiting a dominant concentration of pore volumes below 50 nm. This mesoporous network accelerates the efficient diffusion of TC molecules, thereby improving both adsorption capacity and kinetics by reducing internal mass-transfer resistance [56]. Such mesoporosity is particularly valuable for antibiotics and other pharmaceutical compounds, which are often too large to access microporous materials.

Elemental analysis (Table 2) shows a high carbon content (92.83 wt %), confirming a predominantly graphitic structure conducive to π–π stacking with TC aromatic rings. The low oxygen (0.66 wt%) and nitrogen (1.21 wt%) contents limit competitive water adsorption while still reflecting successful acid-oxidation functionalization. The presence of iron (5.30 wt%) confirms incorporation of Fe_3O_4 nanoparticles, which contribute to surface complexation and electrostatic interactions and impart magnetic recoverability. Thus, the graphitic framework, oxygenated surface functionalities, tailored porosity, and magnetic

Table 2
Physical properties and elemental composition of the adsorbent.

Adsorbent material	BET Surface area (m^2/g)	Average pore diameter (Å)	C (wt %)	N (wt %)	O (wt %)	Fe (wt %)
FMWCNT	385	21.53	92.83	1.21	0.66	5.30

NB: The Fe and O contents represent both Fe_3O_4 nanoparticles and oxygen-containing surface functionalities (-OH, -COOH, -C=O) introduced during acid oxidation.

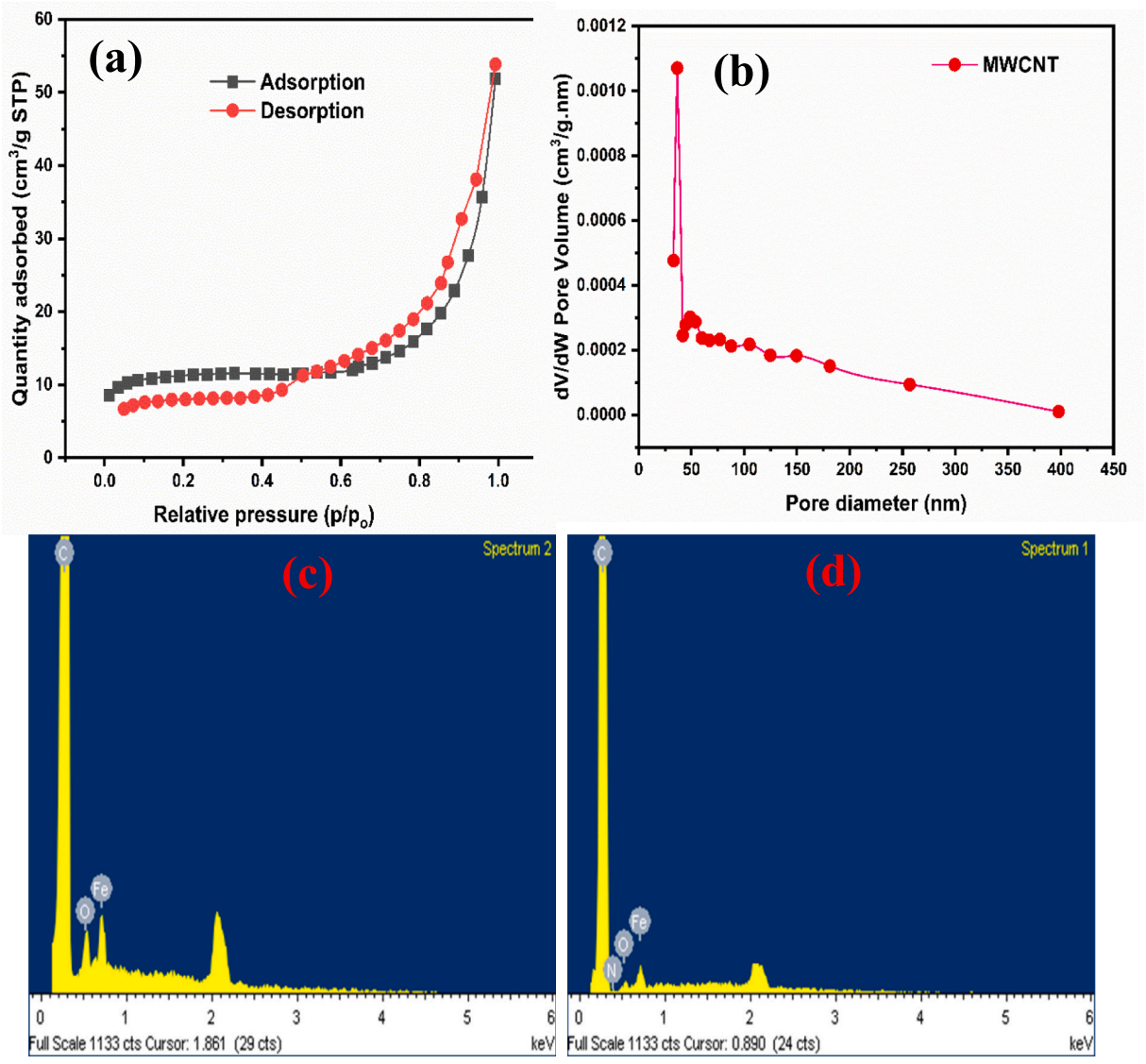

Fig. 3. Nitrogen adsorption-desorption isotherm of MWCNT with H_3 hysteresis loop (a). BJH pore size distribution curve of the synthesized MWCNT (b), Energy-dispersive X-ray spectroscopy spectra of functionalized magnetic carbon nanotubes (FMWCNT) before TC adsorption (c) and after TC adsorption (d).

separability underpin the high adsorption efficiency and reusability of FMWCNTs, highlighting their potential as sustainable adsorbents for pharmaceutical-contaminated waters.

The EDX spectra (Fig. 3c and d) confirm successful TC adsorption onto the FMWCNT surface. After adsorption, a distinct nitrogen (N) signal appears alongside carbon (C), oxygen (O), and iron (Fe) peaks (Fig. 3d), whereas nitrogen is absent in the pristine FMWCNTs (Fig. 3c), directly indicating TC immobilization. The emergence of the N peak, together with an increased oxygen signal, supports the binding of TC molecules rich in amino and hydroxyl groups onto the oxidized FMWCNT surface via π–π interactions and electrostatic attraction [57]. Furthermore, the slightly attenuated Fe signal may indicate partial surface shielding by the TC overlayer, consistent with a molecular coating on the magnetite-doped nanotube substrate.

It should be noted that the Fe:O ratio obtained from EDX does not strictly match the ideal stoichiometry of Fe_3O_4 (3:4), owing to the composite nature of the FMWCNTs. In addition to Fe_3O_4, oxygen contributions arise from surface oxygenated functional groups (hydroxyl, carboxyl, and carbonyl) introduced during acid functionalization. These groups play a critical role in enhancing TC adsorption. Therefore, the elemental composition reflects the coexistence of inorganic magnetic phases and functionalized carbon surfaces rather than a pure Fe_3O_4 phase.

The combined mesoporosity, high BET surface area, and favourable elemental composition underscore the strong potential of FMWCNTs for TC adsorption. The mesoporous network ensures effective molecular accessibility, while the carbon-rich surface promotes strong interactions with TC. Hence, these synergistic features support high adsorption efficiency while enhancing kinetics, selectivity, and reusability, consistent with trends reported for advanced carbon-based adsorbents [31,41].

3.1.5. *Surface functional groups of the adsorbent*

The FTIR spectra of the FMWCNTs before and after TC adsorption (Fig. 4) reveal surface interactions and the contribution of functional groups to the adsorption activity. A comparative analysis reveals significant shifts and alterations in characteristic absorption bands, revealing the dynamic interaction between TC molecules and the synthesized FMWCNT surface. The broad peak discovered around 3426 cm^{-1} before adsorption, attributed to the O—H and N—H stretching vibrations of hydroxyl and amine groups [40], shifted slightly to 3436 cm^{-1} after TC adsorption. This red shift indicates the formation of hydrogen bonds between surface hydroxyl groups on FMWCNTs and the polar functional groups on TC molecules. This is consistent with previous reports that identified similar shifts as a signature of hydrogen bonding in CNT-based adsorption systems [58,59].

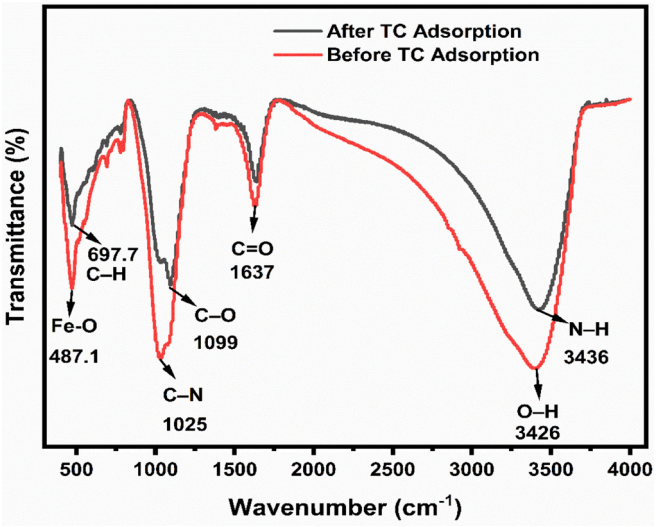

Fig. 4. FTIR Spectra of FMWCNT before and after TC adsorption.

A notable peak was initially found at 1637 cm^{-1}, corresponding to the C═O stretching vibrations of carboxyl or amide functionalities [60] remained visible post-adsorption but showed changes in peak sharpness and slight intensity shifts. This behaviour is characteristic of π–π electron donor-acceptor (EDA) interactions between the delocalized π-electrons of the FMWCNTs and the aromatic rings in the TC structure. Moreover, metal complexation of TC via its keto and enol functional groups with surface-bound Fe_3O_4 (from the catalyst) may also promote this shift [61].

The C—O stretching vibration observed at 1099 cm^{-1} prior to adsorption exhibited a downward shift post-adsorption and a reduction in transmittance. This indicates that ether and phenolic groups on the FMWCNTs actively contributed to binding with TC, possibly via dipole-dipole interactions or hydrogen bonding. Similarly, the band at 1025 cm^{-1}, associated with C—N or C—O bonds [62], also shifted and weakened, strengthening the involvement of these functionalities in the adsorption process.

Also, the low-frequency region revealed prominent changes. The band at 697.7 cm^{-1}, possibly linked to aromatic C—H bending common for TC ring structure or Fe—O vibrations, and 487.1 cm^{-1}, likely attributed to Fe—O (metal–oxygen) stretching, both experienced minor shifts [51]. These changes could point to electrostatic interactions or surface coordination between iron residues on the FMWCNTs and the electron-donating sites of TC.

These observations confirm successful acid-oxidation functionalization of the FMWCNTs, introducing oxygen-containing groups (–OH, –COOH, and –C=O) onto the nanotube surfaces via post-synthesis treatment with H_2SO_4/HNO_3. The introduced functionalities stimulate surface polarity and hydrophilicity, thereby augmenting affinity toward polar and ionizable TC molecules. Corresponding shifts and intensity changes in the FTIR spectra before and after adsorption indicate that TC binding proceeds via multiple concurrent mechanisms, including hydrogen bonding, π–π stacking, electrostatic interactions, and surface complexation, consistent with reports for CNT-based antibiotic adsorbents [63]. The chemical nature of the adsorbent surface, particularly the oxygenated functionalities introduced during acid functionalization, plays a critical role in enhancing these interactions and significantly increasing the adsorption efficiency of FMWCNTs for TC.

3.2. *Optimization of tetracycline adsorption conditions*

The optimization of TC adsorption using FMWCNTs was performed using response surface methodology (RSM) employing a central composite design (CCD). The final second-order polynomial regression model in coded form is given as:

$$\text{TC Removal}\ (\%) = 84.36 - 5.46\,A + 2.51B + 4.39C + 2.90D - 0.9438AB \quad (16)$$

Where A, B, C, and D correspond to adsorbent dosage, pH, contact time, and temperature, respectively. The negative coefficient for A indicates that higher adsorbent dosages may lead to agglomeration or saturation effects, thereby reducing surface area accessibility and diminishing adsorption performance, consistent with findings in carbon-based adsorbent studies [64,65]. On the other hand, positive coefficients for pH (B), contact time (C), and temperature (D) confirm that increasing these variables enhances TC removal under the studied conditions.

The statistical reliability of the quadratic model was substantiated by ANOVA (Table S2), which implied a substantially significant fit ($p = 0.00044$, $F = 4.41$). Adsorbent dosage (A) emerged as the most influential variable ($F = 24.43$, $p = 0.0002$), followed by contact time (C) ($F = 15.23$, $p = 0.0016$) and temperature (D) ($F = 9.09$, $p = 0.0093$). A slight but discernible interaction between pH and dosage (AB) indicated a weak synergistic influence on TC removal. These findings are consistent with previous RSM-based adsorption studies utilizing

functionalized and magnetic nanocomposite adsorbents, where adsorbent loading and contact time were identified as influential variables [40,65]. The favourable role of slightly acidic to neutral pH conditions further correspond to reported TC adsorption behaviour governed by surface charge interactions and amphoteric speciation on oxidized carbon materials [31]. Comparable studies have reported R^2 values exceeding 0.90, supporting the predictive robustness of such regression models [15,64]. The close agreement between predicted and experimental removal efficiencies reinforces the suitability of the model as a practical tool for optimizing operational parameters in scalable TC remediation using magnetically recoverable adsorbents.

3.3. Evaluation of model fitness and predictive performance

The performance of the quadratic model was evaluated using standard fit metrics (Table 3). The mean TC removal efficiency of 82.78%, with low variability (SD = 4.68; %CV = 5.67%), indicates good experimental reproducibility and model stability. The coefficient of determination (R^2 = 0.8151) shows that the model explains a substantial proportion of response variability, while the adjusted R^2 (0.6302) confirms the relevance of the included factors for this multifactor environmental system. Although the negative predicted R^2 (−0.3604) indicates limited extrapolative capability beyond the experimental domain, the model remains suitable for local optimization and process tuning within the defined parameter space.

Although the regression model was statistically significant ($p < 0.05$) and had an acceptable adjusted R^2 (0.6302), the predicted R^2 (−0.3604) signifies limited predictive capability beyond the experimental domain. The divergence between predicted and adjusted R^2 values likely shows experimental variability, model complexity, or the influence of nonlinear interactions and outliers not fully captured by the quadratic model [66].

The experimental domain was constrained to a defined range of operational variables using a central composite design. Within this space, the model adequately fit the data and accurately identified optimal conditions. Validation experiments showed close agreement between predicted and observed removal efficiencies (Table 3), confirming the model's suitability for local optimization. Similar behaviour has been reported in related studies, where models perform reliably within the calibrated range but exhibit reduced accuracy when extrapolated beyond it [64,65].

The model showed adequate precision (9.289), surpassing the recommended threshold of 4.0, indicative of a satisfactory signal-to-noise ratio and suitability for exploring the design space. Although a statistically significant lack of fit was observed (p = 0.0189; F = 7.63), this possibly exhibits inherent experimental variability and system complexity rather than model inadequacy, principally given the model's reproducibility and interpretability within the defined experimental range [40]. Hence, these findings revealed that the quadratic model provides a strong framework for understanding and optimizing TC adsorption on FMWCNTs within the experimental design range.

3.4. Interactive effects of operational parameters on TC removal

Fig. 5(a-f) show the 3D response surface plots obtained from CCD modelling, describing the combined effects of six key variable interactions on TC removal using FMWCNTs. These graphical results provide essential insight into how operational parameters affect adsorption behaviour, enabling fine-tuning of the system for optimal performance. Fig. 5a shows that TC removal efficiency increases with contact time across all pH levels, with the highest removal (90%) observed at ≥90 min and mildly acidic pH levels (5–6). This trend reveals time-dependent saturation of active sites and a favourable TC speciation near its pKa (3.3–7.7), where zwitterionic forms dominate and interact strongly with oxygenated groups on FMWCNTs. At extreme basic or acidic pH, TC solubility and surface protonation undermine adsorption, corroborating findings from other studies [11].

In Fig. 5b, as initial TC concentration rises (10–100 mg/L), removal efficiency declines, especially under alkaline pH conditions. The decline is due to site saturation and weakened electrostatic attraction at elevated pH, where both the TC and adsorbent developed negatively charged. Optimum performance take place at moderate concentrations (50–70 mg/L) and pH 5–6, indicating efficient π–π interactions and hydrogen bonding under these conditions [67].

Fig. 5c shows a rising trend in TC removal with increasing dosage from 0.1 to 0.9 g/L, peak efficiency at higher dosage and pH 6–7. Higher dosages increase available surface area and active binding sites, balancing the loss in adsorption potential that arises under alkaline pH. This confirms the dominant role of both surface functional groups and adsorbent mass in increasing TC uptake, in line with optimization studies on carbonaceous adsorbents [64].

Fig. 5d presents a synergistic interaction where increased dosage and contact time resulted in a rise in TC removal efficiency, attaining a plateau after almost 75 min and approximately 0.75 g/L. This saturation effect indicates the system reaching adsorption equilibrium, after which the contribution of additional adsorbent or time becomes insignificant. Such saturation behaviour aligns with pseudo-second-order kinetics often observed for antibiotic adsorption onto functionalized carbon nanomaterials [68].

Fig. 5e demonstrates that lower TC concentrations require smaller contact times for optimal removal, while elevated concentrations demand lengthy exposure to attain equilibrium. The curve's contour shows diffusion-limited adsorption at higher concentrations, where the time needed for TC molecules to penetrate internal pore networks rises. This interaction supports the dual mechanism of film diffusion and intraparticle diffusion in mesoporous FMWCNTs [69].

Fig. 5f shows that TC removal is highest at low and high adsorbent doses, declining sharply at high concentrations with low adsorbent loading. This strong interaction confirms that site availability is a limiting determinant under high contaminant loads, and adequate dosage is required to maintain removal performance. Notably, more than 0.75 g/L, the dosage effect plateaus, indicating complete utilization of surface-active sites.

Therefore, Fig. 5a–f confirm the predictable and complex behaviour of the FMWCNT system, where adsorption is optimized under mildly acidic pH (5–6), moderate initial concentration (50–70 mg/L), adequate contact time (≥75 min), and high adsorbent dosage (≥0.75 g/L). These interactions highlight the material's adaptability, support the credibility of the statistical model, and strengthen FMWCNTs' suitability for real-world applications targeting emerging contaminants such as TC.

3.5. Perturbation analysis of TC removal efficiency

Fig. S1 illustrates the individual and interactive effects of pH, contact time, adsorbent dosage, and initial TC concentration on removal efficiency. Among these variables, pH has the strongest influence, with optimal TC removal occurring under mildly acidic to neutral conditions, whereas contact time and initial concentration exert moderate positive effects. Adsorbent dosage exhibits the lowest sensitivity, indicating diminishing returns beyond the optimal level. The near-linear trends

Table 3
Summary of model fit for quadratic model data.

Antibiotics	Mean	Std. Dev.	%CV	PRESS	R^2	Pred. R^2	AdjR^2	Adeq Precision	Lack of Fit	p-value	f-value
TC	82.78	4.68	5.67	307.02	0.8151	−0.3604	0.6302	9.289	Significant	0.0189	7.63

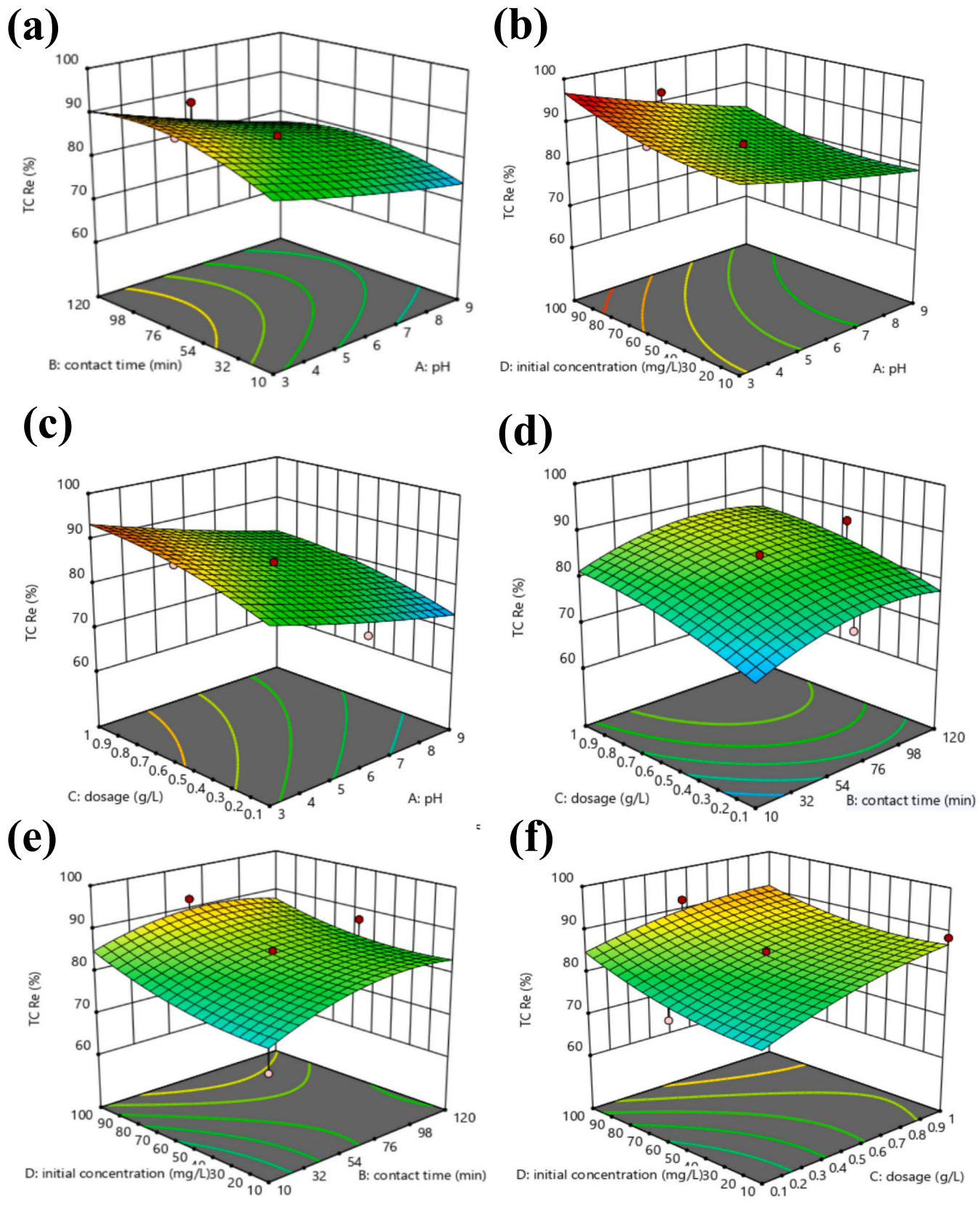

Fig. 5. 3-D response surface plots of pH vs. contact time (a), pH vs. initial concentration (b), pH vs. adsorbent dosage (c), contact time vs. dosage (d), contact time vs. initial concentration (e), and initial concentration vs. dosage (f). The surfaces show optimal ranges, interaction strengths, and plateau regions of TC removal within the CCD-optimized model framework.

confirm that the quadratic model adequately captures the dominant parameter effects without significant higher-order interactions, highlighting pH and contact time as the most critical factors for practical optimization of TC removal.

3.6. pH-dependent speciation and structural insights of TC adsorption

Fig. 6 provides insight into the pH-dependent interaction between TC and FMWCNT. TC speciation as a function of pH, presented in Fig. S1, shows the coexistence of cationic (TCH_3^+), zwitterionic/neutral (TCH_2), and anionic (TC^{2-}) forms, governed by pKa values of 3.33, 7.67, and 9.68. These protonation-deprotonation transitions strongly influence TC's adsorption behaviour by altering its charge state and interaction potential with the FMWCNT surface.

Under acidic conditions, TC predominantly exists in the cationic TCH_3^+ form, which experiences electrostatic repulsion from the positively charged FMWCNT surface, leading to reduced adsorption efficiency. This behaviour is consistent with previously reported observations [41]. As pH increases beyond pKa_1, TC transitions predominantly to the neutral TCH_2 form, which exhibits reduced electrostatic interaction with the adsorbent. Optimal adsorption was observed in the pH range 5–7, where TC is largely neutral, facilitating stronger interactions with the FMWCNT surface through π–π stacking, hydrogen bonding, and residual electrostatic attraction. These findings are consistent with those reported by Zhang et al. [56] and Nguyen et al. [44], who found that neutral pH was most effective for removing antibiotics from aqueous solutions using carbon-derived adsorbents. However, some studies, such as Aliyu et al. [41] reported optimal adsorption at slightly acidic pH for TC, suggesting that the adsorbent surface charge plays a vital role in adsorption efficiency across different pH conditions. The acidic pH zone (below pH 4) typically leads to a decline in adsorption efficacy due to electrostatic repulsion between the adsorbent surface and the positively charged TCH_3^+ species.

The molecular structure of TC, shown in Fig. S1, highlights functional groups governing its protonation behaviour and adsorption interactions. Deprotonation of the phenolic hydroxyl (pKa = 7.67) and carboxyl (pKa = 9.68) groups occurs with increasing pH, while the amino group (pKa = 3.33) remains protonated under acidic conditions. These findings are consistent with [44], where the amino group was found to profoundly impact the binding of TC to adsorbents at low pH. At higher pH levels, the TC^{2-} form (negatively charged) dominates, which improves adsorption via electrostatic attraction with positively charged surface sites on the FMWCNTs [70].

The pH-dependent behaviour observed in this study is consistent with previous studies on TC adsorption using carbon-based adsorbents. As demonstrated by Zhao et al. [10], TC removal was most efficient at pH 5–7, due to the optimal charge of both TC and the adsorbent. Similarly, Topal and Topal [40] and Aliyu et al. [41] reported pH-dependent adsorption trends, with the pH range 5–7 yielding the best interactions between TC and the adsorbent surfaces. Cheung et al. [71] observed that the increase in adsorption capacity at slightly alkaline pH was because of the enhanced deprotonation of TC, which interacts more strongly with the adsorbent surface.

However, optimal pH ranges vary across adsorbents, reflecting differences in functionalization, surface charge characteristics, and adsorption mechanisms. For instance, studies by Katibi et al. [14] and Adeleke et al. [64] suggested that surface oxygenated groups (such as -COOH and -OH) play a significant role in enhancing adsorption at near-neutral pH, in agreement with the findings of this study. Conversely, Ahsan et al. [58] reported a shift in the optimal pH range for different CNT composites, demonstrating the importance of surface chemistry and structural modifications in controlling the adsorption behaviour.

TC adsorption on FMWCNTs is strongly pH-dependent due to TC speciation and the surface charge behaviour of the adsorbent. TC exists in cationic form at pH < 3.3, as zwitterionic species between pH 3.3–7.7, and as anionic forms at higher pH (Fig. S1), while the FMWCNT surface becomes negatively charged above its pH_pzc of 5.19 (Fig. 7). This charge complementarity favors electrostatic interactions with cationic and zwitterionic TC species, resulting in enhanced adsorption at near-neutral conditions. Consequently, optimal TC removal was achieved at pH 5–7, consistent with CNT-based adsorbents reported in the literature and highlighting the importance of pH control for effective pharmaceutical removal.

3.7. Model validation of TC removal under optimized conditions

Table S3 presents the validation of the RSM model utilizing four representative experimental runs. Under optimized conditions (pH 6.5, 400 mg/L FMWCNT, 45 mg/L TC, 23 min), the experimental removal efficiency attained 98.7%, closely corresponding to the predicted value of 98.1% (Δ = 0.6%), validating high model accuracy. When operating conditions deviated from the optimum by increasing TC concentration, reducing the adsorbent dose, or shortening contact time, the model remained robust, with prediction errors below ±1.6%. The close agreement between experimental and predicted values across all runs demonstrates the model's ability to capture nonlinear interactions within the defined operational range.

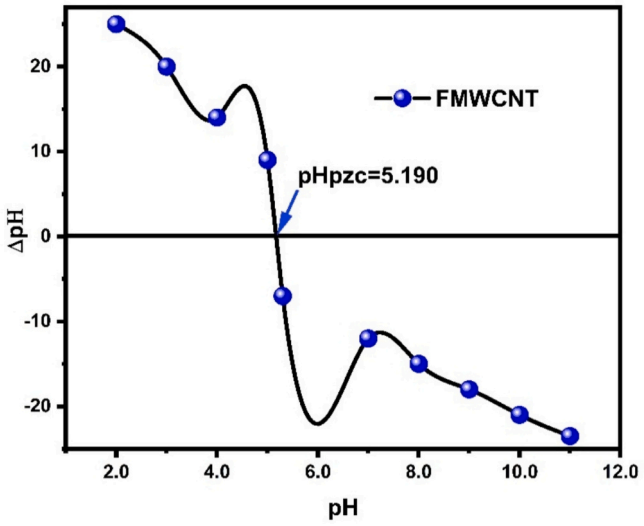

Fig. 6. Point of zero charge (pH_{zpc}) of FMWCNTs using the zeta potential method.

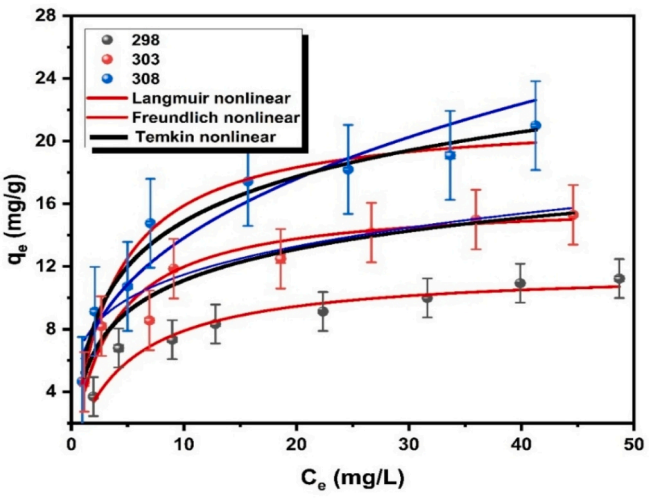

Fig. 7. Nonlinear Langmuir, Freundlich, and Temkin isotherm plots for TC adsorption onto FMWCNT at varying temperatures (298, 303, and 308 K).

These findings validate the statistical reliability and practical relevance of the RSM-based model. The low prediction error (±1.6%) signifies accurate representation of key variables, including pH, adsorbent dose, TC concentration, and contact time. Among these, pH and adsorbent loading were most influential: higher FMWCNT doses increase available binding sites, while mildly acidic conditions stimulate electrostatic and hydrogen-bond interactions with TC. Thus, the validated model provides a robust and cost-effective framework for designing antibiotic removal processes in wastewater treatment.

3.8. Adsorption isotherm and temperature effect on TC uptake

Fig. 7 and Table 4 illustrate the temperature-dependent adsorption of TC onto FMWCNTs (298–308 K) using nonlinear isotherm models. The Langmuir model consistently surpassed the Freundlich model (R^2 = 0.9308–0.9894), indicating predominantly monolayer adsorption on energetically homogeneous sites introduced by surface oxidation. The maximum adsorption capacity (21.67 mg/g) was achieved at 303 K (R^2 = 0.9894), indicating this temperature as optimal due to enhanced molecular mobility and diffusion, which promote π–π stacking and hydrogen bonding. At 308 K, reductions in q_{max} (11.81 mg/g) and kL (0.210 L/mg) suggest partial weakening of adsorbate–adsorbent interactions, consistent with reported destabilization of weak physical forces at elevated temperatures [40].

The Langmuir maximum adsorption capacity (q_m) of FMWCNTs for TC in this research was 21.67 mg/g. Although this value is slightly below that of activated carbon composites such as the DLC@CS adsorbent reported by Singh et al. [72], which achieved a q_m of 29.13 mg/g at neutral pH and 298 K, it is notable that the adsorbent material developed in this study is obtained from steel mill-scale waste via a sustainable, low-cost synthesis route. Compared with other carbon-based adsorbents reported in the literature, FMWCNTs present a practical balance between cost, removal efficiency, magnetic recovery, and regeneration. This supports their practicality for scalable TC remediation applications. The Freundlich model, which accounts for surface heterogeneity and multilayer adsorption, exhibited lower R^2 values than the Langmuir model. Nevertheless, the 1/n values (2.87–4.74) indicate favourable adsorption, while higher k_F values at lower temperatures reflect stronger initial surface affinity. The decline in k_F with increasing temperature suggests reduced interaction strength, plausibly owing to changes in TC speciation and partial disruption of surface hydration.

The Temkin isotherm fit the data well across all temperatures (R^2 = 0.9676–0.9752; Table 4), with the Temkin constant B increasing from 2.153 to 4.130, indicating an endothermic adsorption process. This trend is consistent with enhanced adsorption at moderate temperatures, where thermal energy promotes TC diffusion and its interaction with FMWCNT active sites. Therefore, the Langmuir model provided the best fit, supporting monolayer adsorption on energetically uniform sites, consistent with FMWCNT surface characteristics confirmed by TEM, SEM, and FTIR. The maximum adsorption capacity of 21.67 mg/g at 303 K (R^2 = 0.9894) indicates that this temperature is optimal, underscoring the importance of thermal control for efficient and scalable TC removal.

3.9. Kinetic modelling and mechanistic insights into TC adsorption onto FMWCNT

The adsorption kinetics of TC onto FMWCNT were assessed using nonlinear pseudo-first-order (PFO) and pseudo-second-order (PSO) models (Fig. 8a), with the corresponding kinetic parameters presented in Table 5. At 308 K, the PSO model provided a better fit to the experimental data (R^2 = 0.9393) than the PFO model (R^2 = 0.9095), demonstrating that TC adsorption is more precisely described by the PSO model, which captures both the rapid initial uptake and the subsequent approach to equilibrium. (See Fig. 98.)

Consistent with the superior PSO fit, the predicted equilibrium adsorption capacity (q_e = 122.03 mg/g) surpassed that obtained from the PFO model (108.20 mg/g), signifying that the PSO model more accurately describes the adsorption behaviour and the dominant chemisorption processes involved. The high q_e values are attributable to the large surface area (385 m^2/g), mesoporosity (average pore diameter of 21.53 Å), and abundant surface functional groups (–COOH, –OH) on FMWCNT, which jointly provide superfluous active sites for π–π stacking, hydrogen bonding, and electrostatic interactions with TC [58].

The equilibrium adsorption capacities (q_e) derived from kinetic models represent theoretical maxima under ideal equilibrium settings based on time-dependent adsorption data. Contrastingly, experimental validations under optimized RSM conditions, typically involving operational concentrations and shorter contact times, produced practical q_e values in the range of 45–90 mg/g. The superior performance of the PSO model indicates that TC adsorption onto FMWCNTs is principally governed by chemisorption, involving valence forces and electron sharing or exchange between the functionalized CNT surface and TC molecules. This behaviour is consistent with previous studies on TC adsorption using carbon-based adsorbents, highlighting the importance of surface functionalization and pore accessibility in ascertaining adsorption capacity [62]. Hence, the kinetic analysis confirms that the PSO model most accurately describes the adsorption process.

To further elucidate the adsorption mechanism, the Weber-Morris intraparticle diffusion model was applied by plotting the q_t against $\sqrt{t}$ (Fig. 8b). The resulting multilinear profile reveals that TC adsorption onto FMWCNTs is governed by multiple steps. The initial steep region corresponds to rapid film diffusion, in which TC molecules rapidly occupy external surface sites, followed by a slower linear region associated with intraparticle diffusion within the porous structure. As the linear segment does not pass via the origin, intraparticle diffusion is not the sole rate-limiting step; instead, both film diffusion and pore diffusion contribute to the overall process. The relatively high intercept (C = 41.25) and intraparticle diffusion rate constant (k_{id} = 6.34) indicate a significant boundary-layer effect, while the good correlation coefficient (R^2 = 0.8721) supports the applicability of the model. Thus, these results are consistent with the hierarchical porosity of FMWCNTs, confirming a multistep adsorption mechanism involving both external mass transfer and internal diffusion.

3.10. Thermodynamic analysis of TC adsorption onto FMWCNT

The thermodynamics of TC adsorption onto FMWCNTs were evaluated using a van't Hoff plot of ln K_d against 1/T (Fig. 10; Table S4). The high linearity (R^2 = 0.992) confirms the consistency of the equilibrium data. The positive enthalpy change (ΔH° = +3.92 kJ/mol) indicates a

Table 4
Adsorption isotherm models parameters for TC adsorption on FMWNT.

Adsorbent material	Temperature (K)	Freundlich			Langmuir			Temkin		
		1/n	k_F (mg/g)	R^2	k_L (L/mg)	q_{max} (mg/g)	R^2	A (L/g)	B (J/mol)	R^2
FMWCNT	298	4.74	7.06	0.901	0.285	16.19	0.931	3.64	2.153	0.968
	303	2.87	6.20	0.945	0.276	21.67	0.989	4.78	2.876	0.956
	308	3.26	3.52	0.969	0.210	11.81	0.951	3.66	4.131	0.975

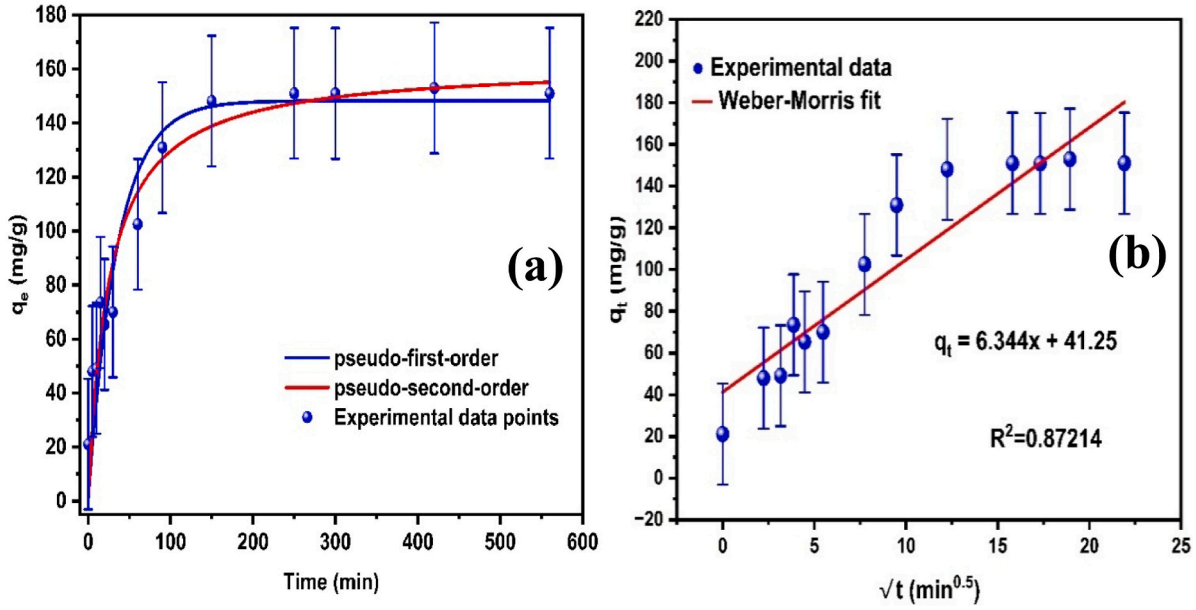

Fig. 8. Pseudo-first-order and second-order kinetic models for the adsorption process (a), Intraparticle diffusion model (Weber-Morris plot) illustrating multi-stage diffusion behaviour (b).

Table 5
Kinetic model parameters for the adsorption of TC onto FMWCNT at 308 K.

Pseudo-First Order			Pseudo-Second Order			Weber-Morris Model		
q_e (mg/g)	K_1 (min^{-1})	R^2	q_e (mg/g)	K_2 (g.mg^{-1} min^{-1})	R^2	C (mg/g)	K_{id} (mg/g·min$^{0.5}$)	R^2
108.20	0.0286	0.9095	122.03	2.4627 × 10^{-4}	0.9393	41.25	6.344	0.8721

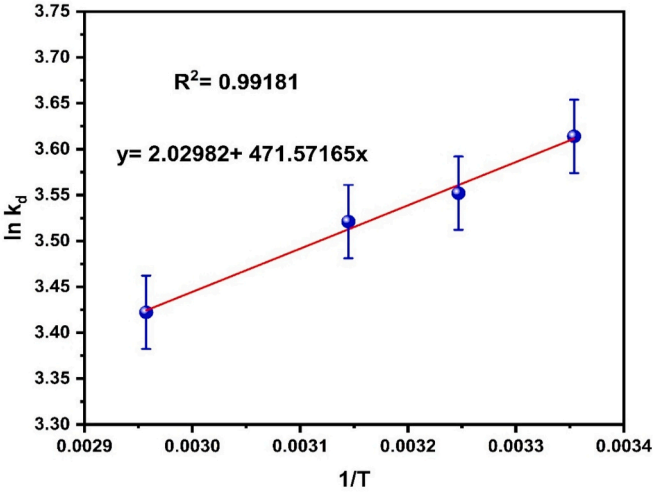

Fig. 9. Van't Hoff plot for TC adsorption onto FMWCNTs showing linear temperature dependency.

mildly endothermic process, consistent with enhanced adsorption at elevated temperatures and the maximum capacity observed at 303 K. Negative Gibbs free energy values ($\Delta G^\circ = -1.11$ to -1.36 kJ/mol) confirm spontaneous adsorption, with increasing favourability at higher temperatures. The positive entropy change ($\Delta S^\circ = +16.88$ J/mol K^{-1}) indicates risen disorder at the solid–liquid interface due to desolvation and surface reorganization during TC adsorption [73].

Synergistically, the entropy-driven and mildly endothermic nature of the process implies that TC adsorption is dominated by low-energy interactions, including electrostatic attraction, π–π stacking, and hydrogen bonding. This behaviour is consistent with adsorption studies of similar antibiotics on carbon-based nanomaterials, where moderate temperature dependence reflects reversible surface interactions rather than strong chemisorption [74,75].

Therefore, the strong alignment between the thermodynamic and kinetic parameters and the isotherm results demonstrates the material's robustness for practical applications. In addition, the low magnitude of ΔG° indicates ease of regeneration, which is highly desirable for reusability in sustainable wastewater purification systems.

3.11. Regeneration and reusability analysis of FMWCNTs

The reusability and long-term stability of an adsorbent are critical for real-world implementation in wastewater purification [30]. The reusability and long-term stability of FMWCNTs were evaluated through four consecutive adsorption–desorption cycles under optimized conditions (0.80 g/L, pH 6.5, 25 °C). As shown in Fig. 10a, TC removal exceeded 95% in the first cycle and declined only slightly to 87% after four successive cyclic tests. This modest loss is attributed to partial desorption, incomplete pore blockage, and gradual depletion of surface oxygenated groups during alkaline regeneration. The slight reduction (8%) highlights the chemical and structural resilience of FMWCNTs and compares favourably with oxidized CNTs and biochars, which typically lose 15–25% capacity within three to five cycles [42,76]. Fig. 10b shows that NaOH-mediated desorption is temperature-dependent, with efficiency rising from 57% at 298 K to 68% at 308 K using 1.0 mol/L NaOH. This trend confirms the endothermic nature of TC desorption, as elevated temperatures increase molecular mobility, weaken surface interactions, and enhance NaOH diffusion within the nanotube network. Notably, enhanced desorption did not compromise subsequent adsorption performance, underscoring the robustness and practical reusability of FMWCNTs for repeated water-treatment applications.

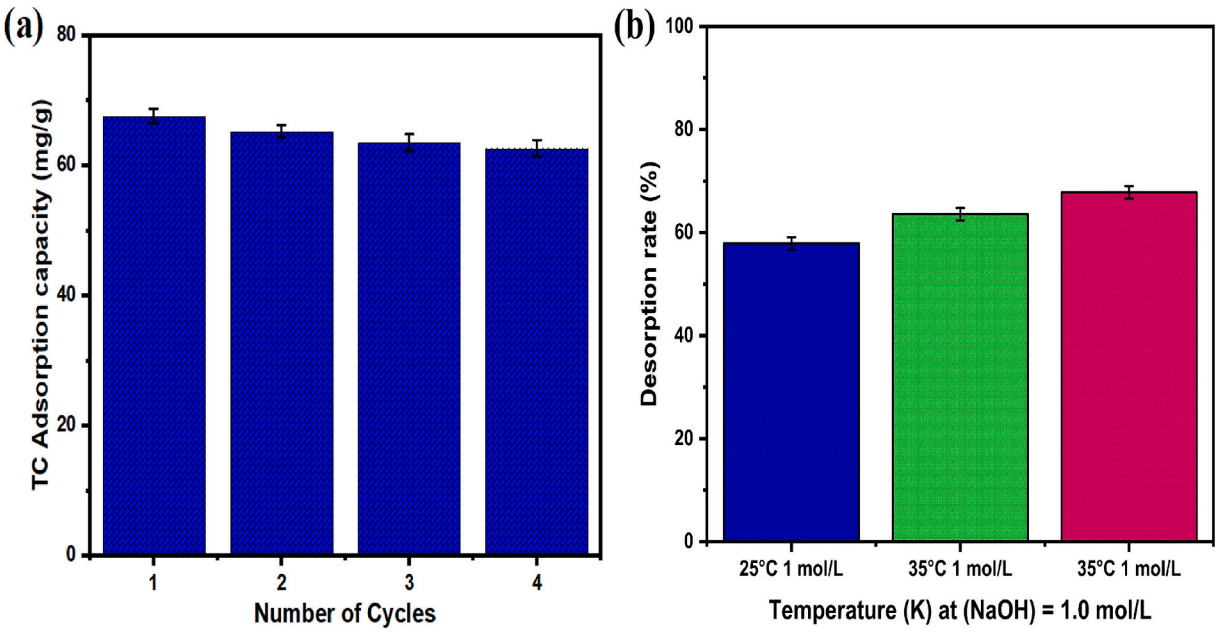

Fig. 10. Reusability study showing TC adsorption efficiency of FMWCNT adsorption-desorption cycles using 1.0 mol/L NaOH, Effect of desorption temperature on TC removal recovery using 1.0 mol/L NaOH (b).

3.12. Comparative assessment of TC adsorption using carbonaceous adsorbents

To contextualize TC adsorption performance, Table 6 compares the iron oxide–loaded FMWCNTs with reported adsorbents. The FMWCNTs exhibit a moderate adsorption capacity (21.67 mg/g), surpassing conventional sorbents such as grape marc–derived activated carbon (6.01 mg/g) and blast furnace slag (15.9 mg/g), though remaining lower than advanced composites such as CNTs–C@Fe–chitosan (192.3 mg/g) and magnetic sludge biochar (145 mg/g). While activated carbon and biomass-derived adsorbents are economically attractive, their practical application is often limited by poor recoverability, regeneration challenges, and difficult post-treatment separation [77]. In contrast, the FMWCNTs developed in this study offer strong operational applicability. Derived from low-cost steel mill-scale waste, they combine the adsorption advantages of nanocarbon materials with facile magnetic recovery, overcoming the cost and separation limitations of conventional CNTs. Although their adsorption capacity is moderate, this is offset by excellent regeneration stability and magnetic retrievability, with 87% efficiency retained after four cycles surpassing more complex systems such as aspartic acid/polypyrrole-functionalized MWCNTs (70%). Unlike many high-capacity composites that require expensive precursors, surfactants, or multi-step synthesis, the surfactant-free, waste-derived FMWCNTs present a more scalable, economically viable, and environmentally sustainable option for practical wastewater purification.

While high-surface-area activated carbons (AC) can demonstrate superior maximum adsorption capacities under highly controlled laboratory conditions [80]. Their widespread practical application is often compromised by significant operational limitations, particularly poor separability and reusability and the energy-intensive challenge of post-treatment separation [74].

The adsorption efficiency of FMWCNTs indicates the synergistic effects of acid functionalization and iron oxide loading. Unlike pristine carbon materials that rely largely on hydrophobic interactions, FMWCNTs have plentiful –COOH and –OH groups and surface Fe^{3+}/Fe^{2+} sites, triggering electrostatic and coordinative binding with TC. Comparative data (Table 6) show that unmodified carbonaceous adsorbents typically exhibit lower uptake and lack magnetic separability, emphasizing the importance of functionalization for improved performance [76]. In addition, FMWCNTs maintained over 87% adsorption efficiency after four regeneration cycles, surpassing many commercial carbons. Together with their sustainable derivation from steel mill-scale waste and rapid magnetic recovery, these features highlight the scalability, durability, and economic viability of FMWCNTs for advanced water purification of pharmaceutical contaminants.

3.13. Plausible TC removal mechanisms using FMWCNT

Multi-technique analysis provides new insight into antibiotic-nanocarbon interactions. FTIR, BET, and EDX results show that TC

Table 6
Benchmark comparison of TC adsorption performance of FMWCNTs with typical carbon-based adsorbents.

Adsorbent material	BET surface area (m^2/g)	TC adsorption capacity/removal	Isotherm model	Kinetic model	Major findings	References
Iron oxide-loaded FMWCNTs (this study)	385	21.67 mg/g	Langmuir	PSO	Mill-scale waste-derived CNTs, magnetic recovery, high reusability	This work
Activated carbon (waste grape marc)	273.9	6.01 mg/g	Langmuir	PSO	Low cost, limited regeneration	[74]
Blast furnace slag	49.3	15.9 mg/g	Langmuir	PSO	Industrial by-product, non-magnetic	[78]
MWCNTs functionalized with aspartic acid/polypyrrole	100.6	34.5 mg/g	NA	NA	Multi-step functionalization	[76]
$MnFe_2O_4$/MWCNTs composite	61.8	83 mg/g (99.2%)	NA	PSO	Magnetic, engineered composite	[42]
CNTs–C@Fe–chitosan composite	6.8	192.3 mg/g	Freundlich	PSO	High capacity, complex synthesis	[79]
Surfactant-modified zeolite	56.3	99.8% removal	Langmuir	PSO	High efficiency, surfactant dependent	[32]

NA = Not available.

adsorption induces the formation of an N/O-rich organic layer on the FMWCNT surface via surface coordination, indicating that removal is governed by specific interactions, particularly Fe–TC chelation and π–π conjugation with graphitic CNT domains [32].

The formation of an interfacial overlayer, coupled with strong electronic interactions, accounts for both the high adsorption efficiency and the stability of the FMWCNT–TC complex. Notably, this surface-sensitive mechanistic insight has not been previously reported for waste-derived, mill-scale magnetic carbon nanostructures. Fig. 11 schematically illustrates the multi-mechanistic adsorption of TC by FMWCNTs, driven by synergistic hydrogen bonding, electrostatic attraction, π–π stacking, and physical entrapment. These mechanisms are consistently supported by FTIR spectral shifts, BET surface-area and porosity changes, pH-dependent adsorption behaviour, surface charge analysis, and microscopic observations.

Hydrogen bonding occurs as a primary contributor to TC uptake [6]. FTIR spectroscopy presents clear evidence for this interaction: the broad N–H/O–H stretching band of FMWCNT (centered around 3426 cm^{-1} prior to adsorption) shifts to 3436 cm^{-1} after TC adsorption [57]. This remarkable red shift indicates the formation of hydrogen bonds between the polar functional groups of TC and surface hydroxyl (and amine) groups on the FMWCNT.

Similarly, the C═O stretching band (1637 cm^{-1}), associated with amide or carboxyl functionalities on the adsorbent, remains visible post-adsorption, but with altered intensity and position [3]. The observed spectral shifts imply that TC's polar groups (hydroxyl, amino, and carbonyl) form specific hydrogen bonds with nitrogen- and oxygen-containing functionalities on the FMWCNT surface. These interactions likely involve polar associations and π–π donor–acceptor effects. Surface functionalization via mild acid oxidation introduces –OH, –COOH, $–NH_2$, and $–OCH_3$ groups, as supported by EDX and prior studies, offering abundant hydrogen-bond donor and acceptor sites [49], facilitating initial sorbent-sorbate anchoring and stabilizing TC at the adsorbent interface.

Electrostatic attraction is an important mechanism that reinforces TC adsorption, which is strongly controlled by solution pH and the charge behaviour of both FMWCNT and TC. The nanotube surface carries a positive charge in acidic conditions (pH < 6.4) and becomes negatively charged in neutral to basic conditions (pH > 6.4) [56]. TC, in turn, is an amphoteric molecule with multiple pKa values (pK_{a1} = 3.33, pK_{a2} = 7.67, pK_{a3} = 9.68), and it transitions via diverse ionic forms with pH: predominantly cationic (TC^+) under low pH, zwitterionic/neutrally charged (TC^0) near pH 5–7, and anionic (TC^-) in more alkaline media [62].

Under highly acidic pH (≤4), TC exists mainly as a cation (TCH_3^+) [75], which is electrostatically repelled by the positively charged FMWCNT surface, leading to poor adsorption. In the near-neutral pH range (6–7), where optimal TC removal was observed, TC exists predominantly in a zwitterionic form, while the FMWCNT surface carries a slight negative charge. This charge complementarity promotes Coulombic attraction, enabling positively charged TC moieties to interact with deprotonated acidic sites on FMWCNTs, whereas negatively charged groups may bind to residual positively charged surface sites. At higher pH (7–8), as the surface develops increasingly negative and TC shifts toward anionic forms, electrostatic interactions may still occur via protonated functional groups or complexation with positively charged Fe sites. However, increasing electrostatic repulsion between TC^- and the negatively charged surface may limit this mechanism's overall contribution [67]. Thus, the pH-dependent uptake trends, low adsorption in strong acid, maximum around neutral pH, and a plateau or slight decline in basic conditions demonstrate the significant role of electrostatic complementarity. The FMWCNT's surface charge characteristics, coupled with TC speciation, elucidate why adsorption is strongest at intermediate pH: herein, electrostatic forces actively draw the TC to the surface, increasing the probability of subsequent π–π and H-bonding interactions once TC is in proximity.

π–π stacking serves as a key binding mechanism between TC and the FMWCNT framework. TC's aromatic rings and conjugated systems align with the delocalized π-electron network on the nanotube sidewalls, enabling strong interactions. The planar geometry of both TC and the graphitic surfaces facilitates this alignment, driven by π–π donor–acceptor interactions and van der Waals forces [3]. Evidence of aromatic stacking was observed in the FTIR spectra: for instance, the absorption band around 1600–1640 cm^{-1} (involving C═C and C═O in aromatic or conjugated domains) changed after adsorption, indicating that π-electron interactions or coordination affected those functional groups [81].

The elemental composition of FMWCNTs reveals a predominantly graphitic carbon structure (93 wt% C), indicating a hydrophobic, aromatic surface well-suited for π–π interactions. This high-carbon framework provides extended regions for TC's aromatic rings to align and π-stack, promoting strong dispersion and π–π binding. Such interactions facilitate effective immobilization of TC and are widely reported in carbon-based adsorbent systems for antibiotic removal [62]. In the present system, they complement other interactions by anchoring TC to the nanotube surface once it diffuses near or contacts the adsorbent.

Physical entrapment (pore-filling effect) of TC within the porous and hollow structure of FMWCNT also plays a critical role in overall uptake. The FMWCNTs exhibit a high specific surface area (385 m^2/g) and a mesoporous structure with an average pore diameter of 2.2 nm, which is well suited for accommodating large organic molecules such as TC. The mesopores and internal cavities of the multi-walled nanotubes facilitate diffusion into internal adsorption sites, enabling effective uptake beyond the external surface. Once inside these pores or inter-tube crevices, TC can be held by pore-filling mechanisms and capillary forces [4]. This is evidenced by the observation that a fraction of adsorbed TC remains firmly or irreversibly bound (unable to be easily desorbed), indicating that some molecules become trapped within the mesoporous framework or in the inner tube cavities. Thus, the high surface area and mesoporous/hollow architecture of FMWCNTs enhance chemical adsorption by providing a reservoir for TC molecules, thereby locking them via spatial confinement in addition to surface bonding.

Importantly, these mechanisms act synergistically rather than independently. The combined effects of hydrogen bonding, electrostatic attraction, π–π stacking, and pore entrapment underpin the high TC removal efficiency (98–99%) observed under optimized conditions. Characterization results consistently support this integrated mechanism, where FMWCNTs immobilize TC through a coordinated interplay of surface interactions. This synergy elucidates the adsorbent's exceptional removal capacity and stability.

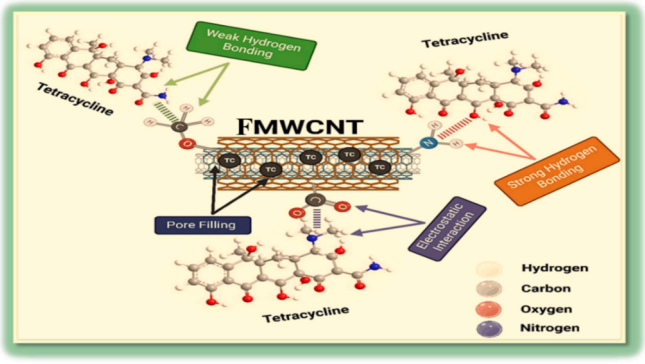

Fig. 11. Proposed TC removal mechanism using FMWCNT adsorbent.

3.14. Application of FMWCNTs to simulated wastewater

To simulate realistic conditions for TC remediation, secondary municipal effluent from Pasar Malam WWTP (Serdang, Malaysia) and

tap water from the UPM Physics Laboratory were spiked to 30 mg/L TC using a standard stock solution. The pH was adjusted to the optimized value (6.5 ± 0.1), and ionic strength was maintained at 0.10 M KCl. FMWCNTs (0.80 g/L) were added, and the mixtures were agitated at 160 rpm and 25 ± 1 °C for 300 min to reach equilibrium. After adsorption, suspensions were filtered (0.22 μm PVDF), and residual TC was quantified at 355 nm by UV–Vis spectrophotometry. All experiments were conducted in triplicate with adsorbent-free controls to account for abiotic losses.

Under these conditions, the FMWCNTs removed 90.5 ± 1.2% of TC from the municipal effluent and 93.3 ± 0.8% from the tap-water matrix (Table S5). These high removal efficiencies in chemically and microbiologically complex waters confirm that the adsorbent's performance is not limited to idealized laboratory solutions. Given its reusability, magnetic recoverability, and derivation from an industrial-waste precursor, FMWCNT represents a sustainable and cost-effective option for remediating pharmaceutical-contaminated water and wastewater.

3.15. Influence of co-existing substances in aqueous matrices

Although this study focused on TC removal under optimized conditions and simulated wastewater, the influence of coexisting constituents in real water matrices warrants consideration. In natural and municipal waters, common anions (SO_4^{2-}, Cl^-), cations (Mg^{2+}, Ca^{2+}), and natural organic matter can compete for adsorption sites or alter surface interactions, potentially affecting adsorption performance. Divalent cations such as Ca^{2+} and Mg^{2+} can compete with TC for negatively charged functional groups on the FMWCNT surface, potentially lowering electrostatic attractions or modifying surface charge [78]. Similarly, higher ionic strength arising from background anions could screen electrostatic interactions between surface sites and TC molecules [67]. NOM, specifically humic substances, may cause additional competition through π-π interactions and hydrogen bonding or cause steric hindrance at the adsorbent interface [82]. While these interferences were not experimentally evaluated in the current work, the proposed adsorption mechanisms suggest that their presence could undermine adsorption efficiency to varying degrees, depending on the matrix and concentration composition. Thus, these considerations highlight the need for future studies that incorporate controlled interferent addition and apply them to real wastewater samples to comprehensively assess adsorbent selectivity and robustness under complex environmental conditions.

4. Conclusion

This study demonstrates that functionalized MWCNT synthesized from steel mill-scale waste are reusable, efficient, and scalable adsorbents for tetracycline removal. Response surface methodology identified pH, contact time, adsorbent dose, and TC concentration as major variables, attaining 98.7% removal under optimized conditions, in close agreement with model predictions. Adsorption followed the Langmuir isotherm (q_{max} = 21.67 mg/g at 303 K) and pseudo-second-order kinetics, controlled by hydrogen bonding, π–π stacking, and electrostatic interactions. The adsorption process was spontaneous and mildly endothermic, and the adsorbent retained 87% of its capacity after four successive regeneration cycles. Entrenched Fe_3O_4 imparted superparamagnetism, facilitating rapid magnetic recovery. Thus, valorizing steel mill waste into FMWCNTs yields a sustainable, efficient, magnetically recoverable adsorbent with strong potential for the practical purification of antibiotic-polluted wastewater.

4.1. Ecotoxicological relevance and environmental significance

By integrating industrial waste valorization with efficient pollutant removal, this study advances sustainable water purification strategies. Acid-functionalized FMWCNTs demonstrate strong potential for mitigating the ecotoxicological risks of tetracycline and associated antibiotics, while magnetic recovery allows efficient separation and reduces secondary pollution. The mechanistic insights elucidate how adsorbent design, mainly surface chemistry, porosity, and magnetism, governs antibiotic binding in complex water matrices, informing the development of eco-benign, next-generation carbon nanoadsorbents. Therefore, the findings of the study are directly relevant to the design of scalable and sustainable technologies for antibiotic sequestration and to the protection of public health and aquatic ecosystems.

CRediT authorship contribution statement

Kamil Kayode Katibi: Writing – review & editing, Writing – original draft, Methodology, Investigation, Conceptualization. **Rabaah Syahidah Azis:** Writing – review & editing, Supervision, Resources, Funding acquisition. **Ibrahim Garba Shitu:** Validation, Software, Data curation. **Ismayadi Ismail:** Project administration, Methodology, Conceptualization. **Muhammad Aliyu:** Writing – review & editing, Writing – original draft, Software. **Nor Kamilah Saat:** Resources, Investigation, Formal analysis, Conceptualization. **Nurul Huda Osman:** Writing – review & editing, Visualization, Validation. **Abiodun Abdulhameed Amusa:** Writing – review & editing, Software, Resources, Formal analysis, Data curation. **Raphael Terungwa Iwar:** Writing – review & editing, Writing – original draft, Visualization. **Abba Mohammed Umar:** Visualization, Software, Formal analysis.

Declaration of generative AI and AI-assisted technologies in the writing process

During the preparation of this work, the author(s) used ChatGPT Plus for basic grammar editing, after which the author(s) assessed the output as needed and took full responsibility for the content of the manuscript.

Declaration of competing interest

The authors declare that they have no known competing financial interests or personal relationships that could have appeared to influence the research reported in this manuscript.

Acknowledgements

The authors are grateful to the Jenis Geran (GP-IPS), Grant No. (GP-IPS/2025/9824000), for funding the project.

Appendix A. Supplementary data

Supplementary data to this article can be found online at https://doi.org/10.1016/j.enceco.2026.02.006.

Data availability

Data will be made available on request.

References

[1] N.T. Padmanabhan, K. Gayathri, R. Mariam, H. John, ZnO/Mo2TiC2 MXene nanohybrids for enhanced solar-driven photocatalytic degradation of tetracycline and organic pollutants in contaminated water, Energy Environ. Sustain. 1 (2025) 100042, https://doi.org/10.1016/j.eesus.2025.100042.
[2] L. Liang, F. Xi, W. Tan, X. Meng, B. Hu, X. Wang, Review of organic and inorganic pollutants removal by biochar and biochar-based composites, Biochar 3 (2021) 255–281, https://doi.org/10.1007/s42773-021-00101-6.
[3] H.U. Cho, H.M. Jang, Investigating the adsorption behavior and mechanisms of swine manure-derived biochar in tetracycline removal, Process. Saf. Environ. Prot. 198 (2025) 107180, https://doi.org/10.1016/j.psep.2025.107180.
[4] J. Zeng, W. Xie, Y. Guo, T. Zhao, H. Zhou, Q. Wang, H. Li, Z. Guo, B. Bin Xu, H. Gu, Magnetic field facilitated electrocatalytic degradation of tetracycline in wastewater by magnetic porous carbonized phthalonitrile resin, Appl. Catal. B Environ. 340 (2024) 123225, https://doi.org/10.1016/j.apcatb.2023.123225.

[5] C. Roderburg, S.H. Loosen, M.S. Joerdens, M. Demir, T. Luedde, K. Kostev, Antibiotic therapy is associated with an increased incidence of cancer, J. Cancer Res. Clin. Oncol. 149 (2023) 1285–1293, https://doi.org/10.1007/s00432-022-03998-z.
[6] K. Naderi, M. Foroughi, M. Hossein, A. Azqhandi, Tetracycline capture from aqueous solutions by nanocomposite of MWCNTs reinforced with glutaraldehyde cross-linked poly (vinyl alcohol)/chitosan, Chemosphere 303 (2022).
[7] C. Shao, J. Zhang, Z. Wang, L. Zhang, B. Wang, J. Ren, X. Zhang, W. He, Photo-Fenton degradation of tetracycline on nitrogen vacancy and potassium-doped Z-scheme FeOCl/NvCN heterojunction with low H2O2 consumption: activity and mechanism, J. Alloys Compd. 970 (2024) 172532, https://doi.org/10.1016/j.jallcom.2023.172532.
[8] Y.H. Chiu, T.F.M. Chang, C.Y. Chen, M. Sone, Y.J. Hsu, Mechanistic insights into photodegradation of organic dyes using heterostructure photocatalysts, Catalysts 9 (2019), https://doi.org/10.3390/catal9050430.
[9] T.O. Ajiboye, L. Sawunyama, M.P. Ravele, A.A. Rasheed-Adeleke, N.H. Seheri, D. C. Onwudiwe, S.D. Mhlanga, Synthesis approaches to ceramic membranes, their composites, and application in the removal of tetracycline from water, Environ. Adv. 12 (2023) 100371, https://doi.org/10.1016/j.envadv.2023.100371.
[10] L. Zhao, Y.G. Zhao, C. Jin, D. Yang, Y. Zhang, M. Progress, Removal of tetracycline by ultraviolet/sodium percarbonate (UV/SPC)advanced oxidation process in water, Environ. Res. 247 (2024), https://doi.org/10.1016/j.envres.2024.118260.
[11] P. Bhatt, C.H. Jeon, W. Kim, Tetracycline bioremediation using the novel *Serratia marcescens* strain WW1 isolated from a wastewater treatment plant, Chemosphere 298 (2022) 134344, https://doi.org/10.1016/j.chemosphere.2022.134344.
[12] K.K. Katibi, K.F. Yunos, H.C. Man, A.Z. Aris, M.Z.M. Nor, R.S. Azis, A.M. Umar, Contemporary techniques for remediating endocrine-disrupting compounds in various water sources: advances in treatment methods and their limitations, Polymers (Basel) 13 (2021) 1–46, https://doi.org/10.3390/polym13193229.
[13] I.G. Shitu, K.K. Katibi, A. Muhammad, I.M. Chiromawa, R.A. Tafida, A.A. Amusa, S. Babani, Effects of irradiation time on the structural, elastic, and optical properties of hexagonal (wurtzite) zinc oxide nanoparticle synthesised via microwave-assisted hydrothermal route, Opt. Quant. Electron. 56 (2024) 1–34, https://doi.org/10.1007/s11082-023-05867-6.
[14] K.K. Katibi, K.F. Yunos, H.C. Man, A.Z. Aris, M.Z.M. Nor, R.S. Azis, An insight into a sustainable removal of bisphenol A from aqueous solution by novel palm kernel shell magnetically induced biochar: synthesis, characterization, kinetic, and thermodynamic studies, Polymers (Basel) 13 (2021), https://doi.org/10.3390/polym13213781.
[15] R.T. Iwar, K. Ogedengbe, K.K. Katibi, L.E. Oshido, Meso-microporous activated carbon derived from raffia palm shells: optimization of synthesis conditions using response surface methodology, Heliyon 7 (2021) e07301, https://doi.org/10.1016/j.heliyon.2021.e07301.
[16] S. Sulaiman, R.S. Azis, I. Ismail, H.C. Man, K.F.M. Yusof, M.U. Abba, K.K. Katibi, Adsorptive removal of copper (II) ions from aqueous solution using a magnetite Nano-adsorbent from mill scale waste: synthesis, characterization, adsorption and kinetic modelling studies, Nanoscale Res. Lett. 16 (2021), https://doi.org/10.1186/s11671-021-03622-y.
[17] K.K. Katibi, I.G. Shitu, R.S. Azis, C. Soo, L.K. Pah, M. Mustafa, A. Kechik, K. F. Yunos, Synthesis of eco-friendly bio-based coconut shell magnetic biochar for efficient bisphenol S sequestration in aqueous environment: green technology breakthrough, Chem. Eng. Commun. 0 (2024) 1–26, https://doi.org/10.1080/00986445.2024.2389134.
[18] X. Shen, X. Jin, F. He, Y. Yang, Corona discharge plasma in collaboration with molecular sieves /Fe degrades tetracycline in water, Chem. Eng. Process. Process Intensif. 219 (2026) 110602, https://doi.org/10.1016/j.cep.2025.110602.
[19] K.K. Katibi, K.F. Yunos, H.C. Man, A.Z. Aris, M. Zuhair, M. Nor, R.S. Azis, A. M. Umar, Contemporary techniques for remediating endocrine-disrupting compounds in various water sources: advances in treatment methods and their limitations, Polymers (Basel) 13 (2021) 3229.
[20] A. Jada, D. Stracke, P. Franco, E.S. Kazan-kaya, Z. Ci, A critical and comprehensive review of the removal of thorium ions from wastewater: advances and future perspectives Zeynep Mine S, J. Water Process Eng. 69 (2025) 106587, https://doi.org/10.1016/j.jwpe.2024.106587.
[21] Z. Seba, N. El Messaoudi, Biosorption of rhodamine B and sunset yellow dyes on cross-linked chitosan-alginate biocomposite beads: experimental and theoretical studies, Int. J. Biol. Macromol. 298 (2025) 139264.
[22] X. Zhao, M. Zheng, X. Gao, J. Zhang, E. Wang, Z. Gao, The application of MOFs-based materials for antibacterials adsorption, Coord. Chem. Rev. 440 (2021) 213970, https://doi.org/10.1016/j.ccr.2021.213970.
[23] X. Zhang, R. Han, X. Gao, C. Jiang, X. Zhao, W. Shi, Liquid-waste derived magnetic porous carbon sphere for effective removal of tetracycline from aqueous solution, Colloids Surf. A Physicochem. Eng. Asp. 687 (2024) 133522, https://doi.org/10.1016/j.colsurfa.2024.133522.
[24] A.A. Oyekanmi, K.K. Katibi, R.C. Omar, A. Ahmad, M. Elbidi, M.B. Alshammari, I. G. Shitu, A novel oil palm frond magnetic biochar for the efficient adsorption of crystal violet and sunset yellow dyes from aqueous solution: synthesis, kinetics, isotherm, mechanism and reusability studies, Appl Water Sci 14 (2024), https://doi.org/10.1007/s13201-023-02060-8.
[25] K. Xu, T. He, L. Li, X. Xing, F. Jiang, J. Iqbal, P. Han, J. Li, DTPA-chitosan mushroom waste biochar for efficient removal of tetracycline from wastewater, Environ. Technol. Innov. 40 (2025) 104472, https://doi.org/10.1016/j.eti.2025.104472.
[26] B. Yang, H. Li, F. Jiang, M. Wang, S. Zhang, K. Liu, Gasification slag–corn root composite for the removal of tetracycline: adsorption performance and mechanism, Biomass Bioenergy 205 (2026) 108583, https://doi.org/10.1016/j.biombioe.2025.108583.
[27] A.A. Alameri, R.H.C. Alfilh, S.A. Awad, G. Sarwar, Z. Tariq, J. Al Musawi, Ciprofloxacin adsorption using magnetic and ZnO nanoparticles supported activated carbon derived from *Azolla filiculoides* biomass, Biomass Convers. Biorefinery 14 (2024) 27001–27014, https://doi.org/10.1007/s13399-022-03372-6.
[28] M. Yilmaz, T.J. Al, M. Morteza, A. Dokht, K. Marziyeh, Synthesis of activated carbon from Lemna minor plant and magnetized with iron (III) oxide magnetic nanoparticles and its application in removal of ciprofloxacin, biomass convers, Biorefinery (2024) 649–662, https://doi.org/10.1007/s13399-021-02279-y.
[29] M. Bassyouni, M.H. Abdel-Aziz, M.S. Zoromba, S.M.S. Abdel-Hamid, E. Drioli, A review of polymeric nanocomposite membranes for water purification, J. Ind. Eng. Chem. 73 (2019) 19–46, https://doi.org/10.1016/j.jiec.2019.01.045.
[30] S.S. Hosseini, A. Hamadi, R. Foroutan, S.J. Peighambardoust, B. Ramavandi, Decontamination of Cd2+ and Pb2+ from aqueous solution using a magnetic nanocomposite of eggshell/starch/Fe3O4, J. Water Process Eng. 48 (2022) 102911, https://doi.org/10.1016/j.jwpe.2022.102911.
[31] H.F. Nassar, A. Shaban, A. Zaher, T. Abdelmonein, E. Salama, Y. Gaber, N. Shehata, R. Abdelhameed, R. Mahmoud, Iron-Trimesic metal organic frameworks as nano-adsorbents for tetracycline and ceftriaxone contaminated wastewater effluents, Egypt. J. Chem. 66 (2023) 439–449, https://doi.org/10.21608/EJCHEM.2022.153568.6647.
[32] F. Kord, M. Yilmaz, A. Hossein, A. Younesi, Adsorptive removal of tetracycline from aqueous solution by surfactant-modified zeolite: equilibrium, kinetics and thermodynamics, Desalin. Water Treat. 247 (2022) 216–228, https://doi.org/10.5004/dwt.2022.27943.
[33] R.T. Iwar, O.T. Iorhemen, K. Ogedengbe, K.K. Katibi, Novel aluminium (hydr) oxide-functionalized activated carbon derived from Raffia palm (*Raphia hookeri*) shells: augmentation of its adsorptive properties for efficient fluoride uptake in aqueous media, Environ. Chem. Ecotoxicol. 3 (2021) 142–154, https://doi.org/10.1016/j.enceco.2021.03.003.
[34] M.U. Abba, H.C. Man, R.S. Azis, A.I. Idris, M.H. Hamzah, M. Abdulsalam, Synthesis of nano-magnetite from industrial mill chips for the application of boron removal: characterization and adsorption efficacy, Int. J. Environ. Res. Public Health 18 (2021) 1–18, https://doi.org/10.3390/ijerph18041400.
[35] M.F. Elmahaishi, R.S. Azis, I. Ismail, F.D. Muhammad, A review on electromagnetic microwave absorption properties: their materials and performance, J. Mater. Res. Technol. 20 (2022) 2188–2220, https://doi.org/10.1016/j.jmrt.2022.07.140.
[36] D.M.S. Prado, G. Li, J.A.D. del Rosario, J.D. Ocon, P. Abel Chuang, Improved oxygen reduction reaction activity of graphene via mechanochemical activation and halogen-doping, ChemElectroChem 12 (2025) e202400494.
[37] O.M. Lemine, Superlattices and microstructures using, XRD line profiles analysis, FE-SEM and FT-IR, Superlattice. Microst. 45 (2009) 576–582, https://doi.org/10.1016/j.spmi.2009.02.004.
[38] M.F. Elmahaishi, R.S. Azis, I. Ismail, M.S. Mustaffa, Z. Abbas, K.A. Matori, F. D. Muhammad, N.K. Saat, R. Nazlan, I.R. Ibrahim, N.H. Abdullah, N. Mokhtar, Structural, electromagnetic and microwave properties of magnetite extracted from mill scale waste via conventional ball milling and mechanical alloying techniques, Materials (Basel) 14 (2021), https://doi.org/10.3390/ma14227075.
[39] M. Bahgat, A.A. Farghali, W.M.A. El Rouby, M.H. Khedr, Synthesis and modification of multi-walled carbon nano-tubes (MWCNTs) for water treatment applications, J. Anal. Appl. Pyrolysis 92 (2011) 307–313, https://doi.org/10.1016/j.jaap.2011.07.002.
[40] M. Topal, E.I. Arslan Topal, Optimization of tetracycline removal with chitosan obtained from mussel shells using RSM, J. Ind. Eng. Chem. 84 (2020) 315–321, https://doi.org/10.1016/j.jiec.2020.01.013.
[41] M. Aliyu, A.H. Abdullah, M.I. bin M. Tahir, Adsorption tetracycline from aqueous solution using a novel polymeric adsorbent derived from the rubber waste, J. Taiwan Inst. Chem. Eng. 136 (2022) 104333, https://doi.org/10.1016/j.jtice.2022.104333.
[42] Y.T. and P.Z, Weigao Zhao, Chenjie Hao, Yiping Guo, Wanfei Shao, Optimization of adsorption conditions using response surface methodology for tetracycline removal by MnFe2O4/multi-wall carbon nanotubes, Water (Switzerland) 15 (2023) 2392 doi:10.3390/w15132392.
[43] F. Jiang, G. Zhu, C. Zhang, B. Yang, Y. Zhang, M. Wang, Reducing agent-enhanced printed circuit board sludge-based Fenton process for the efficient treatment of coking wastewater: performance, optimization and mechanism, J. Environ. Sci. 162 (2026) 332–342, https://doi.org/10.1016/j.jes.2025.04.050.
[44] V.T. Nguyen, T.B. Nguyen, C.P. Huang, C.W. Chen, X.T. Bui, C. Di Dong, Alkaline modified biochar derived from spent coffee ground for removal of tetracycline from aqueous solutions, J. Water Process Eng. 40 (2021) 101908, https://doi.org/10.1016/j.jwpe.2020.101908.
[45] M. Šolic, S. Maletic, M.K. Isakovski, J. Nikic, M. Watson, Z. Kónya, J. Trickovic, Comparing the adsorption performance of multiwalled carbon nanotubes oxidized by varying degrees for removal of low levels of copper, nickel and chromium(VI) from aqueous solutions, Water (Switzerland) 12 (2020) 1–18, https://doi.org/10.3390/w12030723.
[46] M. Nazhipkyzy, P.J.F. Harris, A. Nurgain, R.R. Nemkayeva, Carbon nanotubes synthesized by CCVD method using diatomite and Shungite minerals, Eurasian Chem. J. 24 (2022) 3–11, https://doi.org/10.18321/ectj1143.
[47] M. Sharma, R. Bhatia, I. Sameera, Investigating the impact of carbon source, additives, and temperature in one-step CVD synthesis of MWCNT, Chem. Phys. Lett. 847 (2024) 141358, https://doi.org/10.1016/j.cplett.2024.141358.

[48] B. Liu, Y. Sun, T. Zheng, X. He, P. Wang, J. Wang, Regeneration of carbon nanotube saturated with tetracycline by microwave-ultraviolet system: performance and degradation pathway, Chem. Eng. J. 394 (2020) 124752.
[49] R. Dubey, D. Dutta, A. Sarkar, P. Chattopadhyay, Functionalized carbon nanotubes: synthesis, properties and applications in water purification, drug delivery, and material and biomedical sciences, Nanoscale Adv. 3 (2021) 5722–5744, https://doi.org/10.1039/d1na00293g.
[50] P. Shukla, P. Saxena, D. Madhwal, N. Bhardwaj, V.K. Jain, Electrostatically functionalized CVD grown multiwalled carbon nanotube/ palladium polymer nanocomposite (MWCNT/Pd) for methane detection at room temperature, Chem. Eng. Sci. 264 (2022) 118191, https://doi.org/10.1016/j.ces.2022.118191.
[51] K.K. Katibi, K.F. Md Yunos, H.C. Man, A.Z. Aris, M.Z.M. Nor, R.S. Azis, Influence of functionalized hematite nanoparticles as a reinforcer for composite PVDF-PEG membrane for BPF rejection: permeability and anti-fouling studies, J. Polym. Environ. (2022), https://doi.org/10.1007/s10924-022-02605-z.
[52] M.U. Abba, H.C. Man, R.S. Azis, A.I. Idris, M.H. Hamzah, K.F. Yunos, K.K. Katibi, Novel PVDF-PVP hollow fiber membrane augmented with TiO2 nanoparticles: preparation, characterization and application for copper removal from leachate, Nanomaterials 11 (2021) 1–18, https://doi.org/10.3390/nano11020399.
[53] I.G. Shitu, K.K. Katibi, L.S. Taura, A. Muhammad, I.M. Chiromawa, S.B. Adamu, S. G. Durumin Iya, X-ray diffraction (XRD) profile analysis and optical properties of klockmannite copper selenide nanoparticles synthesized via microwave assisted technique, Ceram. Int. 49 (2023) 12309–12326, https://doi.org/10.1016/j.ceramint.2022.12.086.
[54] M.M.A. Aslam, H.W. Kuo, W. Den, M. Usman, M. Sultan, H. Ashraf, Functionalized carbon nanotubes (Cnts) for water and wastewater treatment: preparation to application, Sustain 13 (2021) 1–54, https://doi.org/10.3390/su13105717.
[55] M.P. Spaolonzi, E.D.V. Duarte, M.G. Oliveira, H.P.S. Costa, M.C.B. Ribeiro, T. L. Silva, M.G.C. Silva, M.G.A. Vieira, Green-functionalized carbon nanotubes as adsorbents for the removal of emerging contaminants from aqueous media, J. Clean. Prod. 373 (2022) 133961, https://doi.org/10.1016/j.jclepro.2022.133961.
[56] Y. Zhang, Z. Huang, X. Fang, Y. Chen, S. Fan, H. Xu, Preparation of magnetic porous biochar through hydrothermal pretreatment combined with K2FeO4 activation to improve tetracycline removal, Microporous Mesoporous Mater. 343 (2022) 112188, https://doi.org/10.1016/j.micromeso.2022.112188.
[57] Y. Su, Y. Zheng, M. Feng, S. Chen, Magnetic Luffa-leaf-derived hierarchical porous biochar for efficient removal of rhodamine B and tetracycline hydrochloride, Int. J. Mol. Sci. 23 (2022), https://doi.org/10.3390/ijms232415703.
[58] M.A. Ahsan, V. Jabbari, M.T. Islam, R.S. Turley, N. Dominguez, H. Kim, E. Castro, J.A. Hernandez-Viezcas, M.L. Curry, J. Lopez, J.L. Gardea-Torresdey, J.C. Noveron, Sustainable synthesis and remarkable adsorption capacity of MOF/graphene oxide and MOF/CNT based hybrid nanocomposites for the removal of Bisphenol A from water, Sci. Total Environ. 673 (2019) 306–317, https://doi.org/10.1016/j.scitotenv.2019.03.219.
[59] Q. Qi, L. Ma, B. Zhao, S. Wang, X. Liu, Y. Lei, C.B. Park, An effective design strategy for the Sandwich structure of PVDF/GNP-Ni-CNT composites with remarkable electromagnetic interference shielding effectiveness, ACS Appl. Mater. Interfaces 12 (2020) 36568–36577, https://doi.org/10.1021/acsami.0c10600.
[60] P.Y. Zhao, H.Y. Wang, G.S. Wang, Enhanced electromagnetic absorption properties of commercial Ni/MWCNTs composites by adjusting dielectric properties, Front. Chem. 8 (2020) 1–9, https://doi.org/10.3389/fchem.2020.00097.
[61] Y. Yin, S. Yang, Z. Jia, H. Zhang, Y. Gao, X. Zhang, H. Zhong, Z. Zhou, X. Zhang, H. Zhou, Magnetic biochar based on furfural residue as an excellent candidate for efficient adsorption of Tetracycline, Bisphenol A, Congo red, and Cr6+, Environ. Sci. Pollut. Res. (2022) 26510–26522, https://doi.org/10.1007/s11356-022-23978-7.
[62] Y. Xiang, Z. Xu, Y. Wei, Y. Zhou, X. Yang, Y. Yang, J. Yang, J. Zhang, L. Luo, Z. Zhou, Carbon-based materials as adsorbent for antibiotics removal: mechanisms and influencing factors, J. Environ. Manag. 237 (2019) 128–138, https://doi.org/10.1016/j.jenvman.2019.02.068.
[63] G.M. Neelgund, E.A. Jimenez, M.D.K. Ray, Ram L, facilitated adsorption of mercury(II) and chromium(VI) ions over functionalized carbon nanotubes, Toxics 11 (2023) 545.
[64] A.O. Adeleke, R.C. Omar, K.K. Katibi, T.T. Dele-Afolabi, A. Ahmad, J.O. Quazim, A. A. Amusa, M.B. Alshammari, Process optimization of superior biosorption capacity of biogenic oyster shells nanoparticles for Congo red and bromothymol blue dyes removal from aqueous solution: response surface methodology, equilibrium isotherm, kinetic, and reusability studies, Alex. Eng. J. 92 (2024) 11–23, https://doi.org/10.1016/j.aej.2024.02.042.
[65] T.L. Adewoye, O.O. Ogunleye, A.S. Abdulkareem, T.O. Salawudeen, J.O. Tijani, Optimization of the adsorption of total organic carbon from produced water using functionalized multi-walled carbon nanotubes, Heliyon 7 (2021) e05866, https://doi.org/10.1016/j.heliyon.2020.e05866.
[66] G. Fang, D. Huang, Z. Wu, Y. Chen, Y. Li, Y. Liu, Effluent quality soft sensor for wastewater treatment plant with ensemble sparse learning-based online next generation reservoir computing, Water Res. X 25 (2024) 100276, https://doi.org/10.1016/j.wroa.2024.100276.
[67] J. He, J. Tang, Z. Zhang, L. Wang, Q. Liu, X. Liu, Magnetic ball-milled FeS@biochar as persulfate activator for degradation of tetracycline, Chem. Eng. J. 404 (2021) 126997, https://doi.org/10.1016/j.cej.2020.126997.
[68] Y.S.S. Al-Faiyz, M. Gouda, Multi-walled carbon nanotubes functionalized with hydroxamic acid derivatives for the removal of lead from wastewater: kinetics, isotherm, and thermodynamic studies, Polymers (Basel) 14 (2022), https://doi.org/10.3390/polym14183870.
[69] N.M. Mubarak, R.F. Alicia, E.C. Abdullah, J.N. Sahu, A.B.A. Haslija, J. Tan, Statistical optimization and kinetic studies on removal of Zn2+ using functionalized carbon nanotubes and magnetic biochar, J. Environ. Chem. Eng. 1 (2013) 486–495, https://doi.org/10.1016/j.jece.2013.06.011.
[70] C. Wang, W. Sun, H. Zhou, X. Sun, Y. Su, C. He, Adsorption of tetracycline by hydrochar derived from co-hydrothermal carbonization of polyvinyl chloride and garden waste: adsorption characteristics and enhancement mechanism, J. Clean. Prod. 467 (2024) 143007, https://doi.org/10.1016/j.jclepro.2024.143007.
[71] G.W. Cheung, H.D. Cooper-Thomas, R.S. Lau, L.C. Wang, Reporting reliability, convergent and discriminant validity with structural equation modeling: a review and best-practice recommendations, Asia Pac. J. Manag. (2023), https://doi.org/10.1007/s10490-023-09871-y.
[72] H. Singh, G. Murugesan, T. Varadavenkatesan, R. Selvaraj, Mitigation of phytotoxicity and enhanced removal of tetracycline from wastewater using magnetic activated carbon derived from *Peltophorum pterocarpum* leaves, Appl Water Sci 15 (2025) 1–18, https://doi.org/10.1007/s13201-025-02614-y.
[73] Y. Li, S. Ma, S. Xu, H. Fu, Z. Li, K. Li, K. Sheng, J. Du, X. Lu, X. Li, S. Liu, Novel magnetic biochar as an activator for peroxymonosulfate to degrade bisphenol a: emphasizing the synergistic effect between graphitized structure and CoFe2O4, Chem. Eng. J. 387 (2020), https://doi.org/10.1016/j.cej.2020.124094.
[74] S. Sağlam, F.N. Türk, H. Arslanoğlu, Tetracycline (TC) removal from wastewater with activated carbon (AC) obtained from waste grape marc: activated carbon characterization and adsorption mechanism, Environ. Sci. Pollut. Res. 31 (2024) 33904–33923, https://doi.org/10.1007/s11356-024-33493-6.
[75] R. Foroutan, S.J. Peighambardoust, P. Latifi, A. Ahmadi, M. Alizadeh, B. Ramavandi, Carbon nanotubes/β-cyclodextrin/MnFe2O4 as a magnetic nanocomposite powder for tetracycline antibiotic decontamination from different aqueous environments, J. Environ. Chem. Eng. 9 (2021) 106344, https://doi.org/10.1016/j.jece.2021.106344.
[76] A. Khazaie, H. Kia, E. Moniri, A. Hessam, M. Miralinaghi, Adsorption modeling of tetracycline removal by multi-walled carbon nanotube functionalized with aspartic acid and poly-pyrrole using Bayesian optimized artificial neural network, J. Taiwan Inst. Chem. Eng. 144 (2023) 104743, https://doi.org/10.1016/j.jtice.2023.104743.
[77] S. Zhou, H. Qi, M. Zhang, A. Maimaiti, Z. Ma, H. Wu, D. Li, W. Wang, Environmental chemistry and ecotoxicology synthesis of magnetic carbon nanotube material through ball-milling for carbamazepine removal from water: a feasible and reliable method, Environ. Chem. Ecotoxicol. 7 (2025) 1496–1505, https://doi.org/10.1016/j.enceco.2025.07.011.
[78] H.S. Rangappa, P.P. Mon, I. Herath, G. Madras, C. Lin, C. Subrahmanyam, Modeling tetracycline adsorption onto blast furnace slag using statistical and machine learning approaches, Sustainability 16 (2024), https://doi.org/10.3390/su16010464.
[79] J. Ma, Y. Zhuang, F. Yu, Facile method for the synthesis of a magnetic CNTs – C @ Fe – chitosan composite and its application in tetracycline removal from aqueous solutions, Phys. Chem. Chem. Phys. 17 (2015) 15936–15944, https://doi.org/10.1039/c5cp02542g.
[80] F. Marrakchi, M.J. Ahmed, W.A. Khanday, M. Asif, B.H. Hameed, Mesoporous-activated carbon prepared from chitosan flakes via single-step sodium hydroxide activation for the adsorption of methylene blue, Int. J. Biol. Macromol. 98 (2017) 233–239, https://doi.org/10.1016/j.ijbiomac.2017.01.119.
[81] H. Wang, X. Lou, Q. Hu, T. Sun, Adsorption of antibiotics from water by using Chinese herbal medicine residues derived biochar: preparation and properties studies, J. Mol. Liq. 325 (2021) 2–10, https://doi.org/10.1016/j.molliq.2020.114967.
[82] S. Wang, L. Li, S. Yu, B. Dong, N. Gao, X. Wang, A review of advances in EDCs and PhACs removal by nanofiltration: mechanisms, impact factors and the influence of organic matter, Chem. Eng. J. 406 (2021) 126722, https://doi.org/10.1016/j.cej.2020.126722.